Suppression of anti-tumor immunity by tumor cell-intrinsic RASD1

Kyu-Hye Chun

Department of Medical Science

The Graduate School, Yonsei University

Suppression of anti-tumor immunity by tumor cell-intrinsic RASD1

Directed by Professor Sungsoon Fang

The Doctoral Dissertation
submitted to the Department of Medical Science,
the Graduate School of Yonsei University
in partial fulfillment of the requirements for the degree of
Doctor of Philosophy in Medical Science

Kyu-Hye Chun

December 2023

This certifies that the Doctoral Dissertation of
Kyu-Hye Chun is approved.

[Signature]

Thesis Supervisor : Sungsoon Fang

[Signature]

Thesis Committee Member#1 : Jae-woo Kim

[Signature]

Thesis Committee Member#2 : Jae-Ho Cheong

[Signature]

Thesis Committee Member#3: Ho-Geun Yoon

[Signature]

Thesis Committee Member#4: Eun Ji Nam

[three signatures total in case of Master's]

The Graduate School
Yonsei University

December 2023

ACKNOWLEDGEMENTS

I would like to express my heartfelt gratitude to everyone who contributed to the completion of my dissertation and supported me throughout my academic journey.

A sincere thank you to Professor Jae-woo Kim, whose endless support and guidance throughout my Ph.D. journey allowed for quality time together. Your mentorship has guided me through this academic endeavor, made me feel fulfilled. I am truly grateful for the opportunity to have learned from you.

I also want to express my appreciation to Professor Sungsoon Fang for your guidance during my dissertation. Your insight made me shape up nicely and your passion played a crucial role in my Ph.D journey. to Your encouragement and advice have been invaluable, and I am thankful to have an opportunity to learn from someone as dedicated as you.

To Professor Jae-Ho Cheong, I am grateful for your consistent interest and assistance in my research. Your support and guidance have been instrumental, and I have learned a lot from your expertise and enthusiasm for research. Also, I would like to express my sincere gratitude to Professor Ho-Geun Yoon and Professor Eun ji Nam, my dissertation advisor, for their warm advice and guidance throughout my degree program.

Professor Ji Hyung Chung, your unwavering support and guidance in my degree program have been invaluable. Your endless encouragement has been a source of strength allowing me to shine. I would like to extend my appreciation to the members of the Biochemistry and Molecular Biology department, including

Professors Kyung-sup Kim, Sahng Wook Park, and Kyung-Hee Chun, for their interest in my research and for their meaningful discussions during research seminars.

To Dr. Mi-Young Kim and Dr. Tae-Hyun Kim, I am thankful for your invaluable guidance and advice, especially during challenging moments. I am also fortunate to have met Dr. Bo Kyung Yoon, whose warmth and support have been invaluable. Thank you so much for being a good senior and a sister and thank you for guiding me well.

To Dr. Nahee-Hwang, thank you for being a good colleague throughout my degree process. Yoseob Lee, thank you for being so considerate and always helping me out. To Hyeonuk Jeon, thank you for being kind. Hyunsik Kim, thank you for being a great friend and always being on my side. Jae-Hwan Kwon and Chansik Kim, thank you for making enjoyable memories together. Dr. Hyeok-Gu Kang, thank you for willingly sharing your experimental knowledge with me. Dr. Hyeonhui Kim, thank you for helping me with my experiments whenever needed. To Sugyeong Jo and Chae Min Lee, thank you for your support and friendship during overtime hours.

Lastly, to my family, I wouldn’t have done it without your support. To my grandfather, Hai-Soo Chun, who always keeps an eye on my research; my dad, Byung-Hee Chun, who always comes late at night to pick me up; my mom, Seung-Hee Kang, who cooks delicious food to cheer me up; my best buddy, Kyu-Yeon Chun, whom I love and rely on the most; and my brother-in-law, Sunjoong Kim, I am thankful to be with you. I was able to do all of these because of my family. I love you all and thank you.

<TABLE OF CONTENTS>

LIST OF FIGURES

ABSTRACT

Suppression of anti-tumor immunity by tumor cell-intrinsic RASD1

Kyu-Hye Chun

Department of Medical Science
The Graduate School, Yonsei University

(Directed by Professor Sungsoon Fang)

Glucocorticoid receptor signaling pathway is essential for inhibition of the immune responses by repressing the transcription of genes related to inflammation. Synthetic glucocorticoids, such as dexamethasone, are utilized for their immune suppressive properties in arthritis, allergic reactions, and immune system disorders. Here, I suggest RASD1 (also known as Dexras1, Dexamethasone-induced Ras-related protein 1), a target gene of glucocorticoid receptor signaling pathway, as a key mediator of immune suppression, influencing immunotherapy response and possessing the potential role as a biomarker. Transcriptomic analysis of gastric cancer cells, down-regulation of RASD1 enhances the anti-tumor immune response. Ablation of RASD1 upregulates CSF2, a target gene of the NF-κB signaling pathway. CSF2 stimulates cytokine production and promote the differentiation of proinflammatory macrophages. An in vivo study using a syngeneic mouse model found that elevated RASD1 expression levels in cancer cells is correlated with larger tumor size and resistance to immune checkpoint blockade. Further study identified that RASD1 interacts with BRD4, inhibiting CSF2 transcription at the promoter region, thereby blocking the activation of NF-κB signaling pathway and reducing the inflammatory response against cancer cells. CSF2 and anti-PD1 were intraperitoneally injected to mice bearing the tumor derived from RASD1-overexpressing cancer cells exhibited anti-tumor effects. Furthermore, high RASD1 expression in gastric cancer patients was associated with poor immunotherapy

response rates and reduced pro-inflammatory macrophages in immunotherapy non-responder group. These results indicating that RASD1 serve as a potential prognostic biomarker for immunotherapy. This study provides valuable insights into the role of RASD1 in immune suppression in tumors, contributing to a better understanding of the tumor microenvironment and offering novel therapeutic resume.

Key words: gastric cancer, rasd1, immune suppression, immunotherapy, biomarker

Suppression of anti-tumor immunity by tumor cell-intrinsic RASD1

Kyu-Hye Chun

Department of Medical Science
The Graduate School, Yonsei University

(Directed by Professor Sungsoon Fang)

I. INTRODUCTION

Gastric cancer, a common malignancy with molecular diversity, ranks fifth in incidence and third in cancer-related deaths worldwide[1]. Current treatments predominantly involve surgery and chemotherapy. Notably, the MAGIC trial showed a significant increase in the 5-year survival rate of patients who received perioperative chemotherapy compared to patients undergoing surgical resection alone (36% vs. 23%)[2]. However, for gastric cancer with regional metastasis, the survival rate after chemotherapy drops to 6.7%. The chemotherapy regimens including 5-fluorouracil, folinic acid, oxaliplatin, and docetaxel, necessitate further research to address the treatment of cancers that exhibit resistance to these cytotoxic drugs[3]. A prior study highlighted the lack of benefits from fluorouracil-based adjuvant chemotherapy in gastric cancer, identifying a subgroup that did not benefit from chemotherapy[4]. Among these studies, gastric cancer molecular subtypes were classified to predict chemotherapy effectiveness. Among these subtypes, the subtype with low immune response and stem-like properties poses the most challenge to treat, not responding to anticancer drugs and has the lowest survival rate. The stem-like subtype shares similar characteristics with diffuse-type cancer. Gastric cancer can be histologically categorized into intestinal type and diffuse type[5]. Morphologically, the intestinal type shows bulky tumors and has a glandular structure. On the other hand, the diffuse type is characterized by infiltrative

features, and it is primarily observed in young women[6]. Consequently, diffuse-type gastric cancer is known for its high expression of the estrogen receptor, a nuclear receptor. Another characteristic is its high EMT properties and its resistance to immunotherapy. Therefore, a novel therapeutic regimen is needed to treat this type.

Cancer immunotherapy, a third-generation treatment, harnesses the patient's immune system to achieve therapeutic effects, in contrast to traditional anticancer drugs. Immune checkpoint blockade (ICB) therapies, such as monoclonal antibodies against PD-1, PD-L1, or CTLA-4, have been shown to prolong the survival of a subset of patients with melanoma, non-small cell lung cancer, renal-cell cancer, and other cancer types. Immune checkpoints are physiologically important mechanisms for regulating T cells. Inhibition of PD-1/ CTLA-4 on T cell surfaces can be triggered by ligands/receptors on antigen-presenting cells and tumor cells to modulate T cell responses. Although many trials have demonstrated improved overall survival for patients treated with the anti-PD-1 monoclonal antibody in gastric cancer, most gastric cancer patients have a response rate of 10-26% with no selective biomarker or PD-L1. For this reason, to enhance the efficacy of anti-PD1 therapy in gastric cancer, identifying precise predictive biomarkers is essential for selecting patients who would benefit most from immunotherapy.

We aimed to identify a predictive biomarker for immunotherapy response through the glucocorticoid receptor. Glucocorticoids are first-line antiemetics that are administered during platinum-based chemotherapy regimens. Glucocorticoid act via the glucocorticoid receptor (GR), also known as nuclear receptor subfamily 3 group C member 1 (NR3C1). GR binds to glucocorticoid response elements (GRE) in gene promoters, activating their transcription. GR induces or represses the transcription of target genes that are involved in inflammation and immune response. Therefore, synthetic glucocorticoid such as dexamethasone are widely used for their anti-inflammatory and immune-suppressive properties in managing symptoms, including

cancers. Previously, we have shown RASD1's involvement in adipogenesis[7], osteogenesis[8], and IGF-1 signaling[9]. RASD1, a member of the Ras family of G-proteins, has emerged as a significant player that is induced by glucocorticoids.

Our investigation sought to determine if RASD1, a target gene of GR, contribute to immune suppression in cancer. Furthermore, by analyzing the transcriptome profile, we uncovered that RASD1 knockdown triggers inflammatory responses. Tumor-infiltrating lymphocytes (TILs) from RASD1 overexpressed tumors shows enrichment of M2 macrophage phenotype. Moreover, RASD1 ablation leads to CSF2 transcription, converting M2 macrophages into M1 macrophages and promoting an inflammatory tumor environment.

This study highlights, RASD1 not only as a potential predictive biomarker but also as a promising therapeutic target for immunotherapy in gastric cancer. Considering the unfavorable prognosis linked to high RASD1 expression, our results suggest that targeting RASD1 overexpressed tumors with myeloid-targeted immunotherapy could synergize with immune checkpoint blockade therapies. RASD1 holds promise as a biomarker in this context.

II. MATERIALS AND METHODS

1. Clinical cohort

All fresh frozen tumor tissues and clinical data were collected at Yonsei Cancer Center (Seoul, Republic of Korea) from gastric cancer patients who underwent curative intent gastrectomy. All experimental procedures were approved by the institutional review board of Severance, and all participants provided written informed consent. We generated multiple batches of cohort dataset through the samples (n=497; GSE13861 and GSE84437; Illumina HUmanHT-12 v3.0 Expression BeacChip array).

2. TCGA dataset

The normalized tumor sample RNA sequencing data expression patterns from TCGA STAD were downloaded from cBioportal.

3. Cell culture

All gastric cancer cell lines (Hs746T, MKN1, SNU668, SNU601, YCC7, and NCIN87) were obtained from the Korean Cell Line Bank (KCLB). MC38 mouse colon adenocarcinoma cells were obtained from Kerafast (Cat. ENH204-FP, Boston, MA), and CT26 mouse colon carcinoma cells were obtained from ATCC (Cat. CRL-2638). HS746T, YCC7, and MC38 cells were grown in Dulbecco's modified Eagle medium (DMEM) (Gibco) with 10% fetal bovine serum (FBS), 2mM L-glutamine, 100 U/ml penicillin, and 100 μg/ml streptomycin. MKN1, SNU668, SNU601, CT26 and 4T1 cells were grown in RPMI1640 (Hyclone) with 10% fetal bovine serum (FBS), 2mM L-glutamine, 100 U/ml penicillin, and 100 μg/ml streptomycin. All cells were cultured at 37℃ in a humidified atmosphere containing 5% CO2 and regularly tested for mycoplasma contamination.

4. Lentivirus stable cell line

To generate stable cell lines, pLKO.1-TRC, psPAX2, and pMD2.G vectors were mixed with FuGene (Promega) in Opti-MEM (Gibco) following the manufacturer's instructions. The mixture was then added to ~80% confluent HEK293T cells with 6ml DMEM growth medium. After 48hours of transfection, the packaged recombinant lentivirus was harvested from the cell supernatant and added to Hs746T, MC38, and CT26 cells. Following 24 hours of incubation, puromycin selection was conducted for 7-10 days before expansion of the stable cell lines. The target sequences for shRNAs were as follows: (human) shRASD1: CGACACCAAGTCTTGCCTCAA;(mouse) shRASD1:GACCTCATGTACATTCGTGAA; non-targeting control (SHC002). The RASD1-expressing MC38 and CT26 cell lines were established using pLJM1-EGFP vectors obtained from Addgene (plasmid 19319). The pLJM1-EGFP, psPAX2 and pMD2.G vector mix was added to HEK293T cells. GFP expression was observed by fluorescent microscopy after 24hours, and the packaged recombinant lentivirus was harvested from cell supernatant after 48hours of transfection. The virus-containing supernatant, after filtration, was added to the MC38 and CT26 cell lines. Puromycin selection of stable clones was carried out for two weeks.

5. Bulk RNA sequencing

Total RNA concentration was calculated using the Quant-IT RiboGreen assay (Invitrogen, #R11490). To assess the integrity of the total RNA, samples were run on the TapeStation RNA screentape (Agilent, #5067-5576). Only high-quality RNA preparations, with an RNA Integrity Number (RIN) greater than 7.0, were used for RNA library construction. A library was independently prepared with 1ug of total RNA for each sample using the Illumina TruSeq Stranded mRNA Sample Prep Kit (Illumina, Inc., San Diego, CA, USA, #RS-122-2101). The first step in the workflow involved purifying the poly-A containing mRNA molecules using poly-T-attached magnetic beads.

Following purification, the mRNA was fragmented into small pieces using divalent cations under elevated temperature. The cleaved RNA fragments were copied into first-strand cDNA using SuperScript II reverse transcriptase (Invitrogen, #18064014) and random primers. This was followed by second-strand cDNA synthesis using DNA Polymerase I, RNase H and dUTP. These cDNA fragments then underwent an end repair process, the addition of a single 'A' base, and ligation of the adapters. The products were then purified and enriched with PCR to create the final cDNA library.

6. RNA extraction and quantitative PCR

mRNA expression levels were assessed using real-time PCR. Total RNA was extracted using the TRIzol reagent (Invitrogen) following the manufacturer's instructions. RNA was subjected to cDNA synthesis with random hexamer primers using Superscript Ⅱ reverse transcriptase (Invitrogen). Quantitative RT-PCR (qRT-PCR) was performed with SYBR Green PCR Master Mix (Applied Biosystems) using an ABI PRISM7300 RT-PCR system (Applied Biosystems). All experiments were performed in biological triplicate and normalized into 36B4 expression. The 2-ΔΔCt method was used for quantification. The following primers were used: For mouse RASD1: Forward 5'-TGCACAAGAAGGCTCTGAGG-3', Reverse 5'-CACAGCGCTCCTTGTCCTTA-3'. For human RASD1: Forward 5'-AGCTGAGTATCCCGGCCAA-3', Reverse 5'-CGATGGTAGGCGTGTAGGC-3'.

7. Luciferase assay

p65RE x 3 and pGL3-CSF2 luciferase reporter plasmid containing the SV40 mini promoter were used for assay. Luciferase reporter plasmids were transfected into HEK293T cells together with GFP-p65, GFP-BRD4, pCNS-D2-RASD1 plasmids. Beta-galactosidase serves as an internal control, normalizing luciferase activity for variations in transfection efficiency.

8. Chromatin immunoprecipitation assay

293T cells were seeded at density of 1 x 106 and attach for 24 hours (using 150 x 20 mm TC dishes). Cells were transfected with pCNS-D2-RASD1 vectors using PEI and subjected to chromatin immunoprecipitation (ChIP) analysis using Pierce Agarose ChIP Kit (Thermo, 26156) using 1% formaldehyde for crosslinking. Cell lysates were sonicated to shear DNA to an average fragment size of 150-500bp. The sonicated chromatin was immunoprecipitated with normal IgG, and antibodies for NF-KB (Santacruz, sc-8008), BRD4 (Cell signaling,13440) incubated with Protein A/G Plus Agarose beads (Santacruz, sc-2003) at 4°C for overnight. Agarose beads were extensively washed, and protein-DNA cross-links were reversed and eluted. DNA was extracted from the immunoprecipitants and analyzed by quantitative PCR. The following primers were used: PD-L1: Forward 5'-GAAGGTCAGGAAAGTCCAAC-3', Reverse 5'-TCGGGAAGCTGCGCAGAACT -3'

9. Immunoprecipitation

Immunoprecipitation assays were performed using Cell lysis buffer (50mM Tris-HCl, 150 mM NaCl, 0.2% Triton X-100, 0.3% NP40) containing Protease Inhibitor cocktail. Cell lysates were incubated with the indicated antibodies at 4°C overnight. The protein complex was captured using protein A/G plus agarose beads (Santacruz, sc2003) were collected by centrifuge and washed three times with washing buffer. The precipitated proteins were mixed with 5X SDS-PAGE loading buffer (Biosesang, SF2002-110-00) and subjected to western blot analysis. The following primary antibodies were used for IP: 6X His (Invitrogen, MA1-21315), GFP (Santacruz, sc9996), GAPDH (Cell signaling, 2118S).

10. Western blot analysis

Cells were lysed with 1% SDS-containing buffer for protein extraction. Protein

quantification was performed using the BCA assay kit (Thermo Fisher Scientific, MA, USA). Equal protein amounts were loaded onto SDS-PAGE gels and transferred to nitrocellulose membranes. Western blot analysis was completed with following antibodies: NF-κB p65 Ab (Santacruz, sc-8008), BRD4 Ab (Cell Signaling, 13440), RASD1 Ab (Cell Signaling, 4229), GAPDH Ab (Cell signaling, 2118S). Membranes were blocked with 5% fat-free milk for 1 h and incubated with primary antibodies at 4 °C overnight. After washing with TBST, membranes were incubated with corresponding secondary antibodies at room temperature for 1 h and washed to remove non-specific bindings. Target protein expression was visualized using the ECL detection system (Thermo, 34580).

11. Cell counting kit-8 (CCK-8) assay

The MC38 and CT26 cells were plated in a 12 well plate (1×10^4cells/well). To quantitively evaluate the viability of cells, the medium in each well was replaced by medium containing 10% CCK-8, and cells were incubated at 37°C for 30minutes. The absorbance weas calculated at wavelengths of 450nm using microplate reader (Bio-Rad, USA). Cells were counted every 24, 48, and 72 hours.

12. Immunofluorescence

HS746T cells were seeded at density of 1×10^5 cells onto glass coverslips in 12-well plates. After fixation with 3.7% PFA, permeabilization with 0.2% Triton X-100, and blocking with 1% BSA, cells were incubated overnight at 4°C with anti-RASD1 antibody (Abcam ab251924) followed by fluorescent secondary antibody. Imaging and analysis were performed using a Zeiss LSM-780 microscope with Airyscan processing (ZEN2.3 software).

13. In vivo animal studies

C57BL/6J, BALB/c and BALB/c nude mice (female, 7 weeks old) were purchased from the Jackson Laboratory. All mice were maintained in pathogen-free animal housing. To develop tumors, 2 x 10^5 lentiviral control and target-gene cells were implanted subcutaneously in the right flank. Tumor volume was measured using a caliper every 2-3 days and estimated using the following formula: $L \times W^2/2$, where L=Length, W=Width, and $L > W$. The maximum tumor size allowed by the institutional ethical board is 2000 mm^3. Mice were treated with either 100μg/mouse isotype control antibody (Bio-X-Cell, BE0089) or checkpoint blockade antibody (Bio-X-Cell, BE0146) injected intraperitoneally on day 4, 7, and 10. And for recombinant murine GM-CSF (20ng/ml; Peprotech) was used. Mice were randomized into groups based on the average tumor volume using the formula above. All animal experiments were performed in compliance with ethical guidelines and approved by the Yonsei University Health System Institutional Animal Care and Use Committee (IACUC).

14. Mouse tumor infiltrating lymphocytes isolation

For scRNA-seq analysis of immune cells from MC38 tumors, the tumors were mechanically minced and digested with Collagenase Type I (Gibco, 250U/ml) and DNase Ⅰ (Roche, 20U/ml) for 30minutes at 37°C. The dissociated cells were passed through a 70-μm cell strainer (SPL) and washed twice with DMEM containing 10% FBS. Single-cell suspensions were stained with PE-CD45 (Biolegend, 103105) for 30 minutes at 4°C. Dead cells were excluded using the Live/Dead Fixable Aqua Dead Cell Stain Kit (Invitrogen, L34965). The positive fraction of TILs was sorted with a BD FACS Aria Ⅱ.

15. Single cell RNA-sequencing and library preparation

MC38 tumors were harvested from a syngeneic mouse model (n=6 per group). The cell count in the suspensions was determined using the LUNA-FL™ Automated Fluorescence Cell Counter (logos biosystems). For more information on preparing cells, the 10x Genomics Single Cell Protocols Cell Preparation Guide and the Guidelines for Optimal Sample Preparation flowchart (Documents CG00053 and CG000126, respectively) were consulted. Libraries were prepared using the Chromium controller according to the 10x Chromium Next GEM Single Cell V(D)J User Guide (CG000331). Briefly, the cell suspensions were diluted in nuclease-free water to achieve a targeted cell count of 10,000. The cell suspension was mixed with master mix and loaded with Single Cell 5′ Gel Beads and Partitioning Oil into a Next GEM Chip K. RNA transcripts from single cells were uniquely barcoded and reverse-transcribed within droplets. cDNA molecules were pooled and enriched with PCR. For V(D)J Enriched Library, the enriched cDNA pool was first amplified using T Cell Mix1 primer or B Cell Mix1 and then second amplified using T Cell Mix2 primer or B Cell Mix2 primer. For the 5' Gene Expression Library, the cDNA pool underwent an end repair process, the addition of a single 'A' base, and then ligation of the adapters. The products were then purified and enriched with PCR to create the 5' Gene Expression Library. The purified libraries were quantified using qPCR according to the KAPA qPCR Quantification Protocol Guide and qualified using the Agilent Technologies 4200 TapeStation. Finally, the libraries were sequenced using HiSeq platform (Illumina) according to the read length specified in the user guide.

16. Flow cytometry

Tumors were collected and enzymatically digested to obtain single-cell suspension, which were then filtered twice through 70μm filters. Red blood cells were lysed and washed with Cell Staining Buffer (Biolegend). The filtered cells were then blocked with an anti-CD16/32 antibody and stained with indicated surface antibodies for 20min on ice.

Dead cells were marked using live/dead fixable Aqua dye (Thermo). The following antibodies were used: anti-CD45 PE, anti-CD3 PerCP/Cy5.5, anti-CD8a PE/Cy7, anti-CD4 Alexa Fluor700, anti-IFNγ APC, anti-CD206 AF647, anti-CD80 APC/Cy7 (all purchased from Biolegend). After resuspending the cells in pre-cold PBS, the suspension was analyzed on BD Verse I. The FACS data were analyzed using FlowJo X V10.

17. Bioinformatics

The GSVA (V1.38.2) software package, available from R/Bioconductor, was used for this study serving as a non-parametric, unsupervised method for estimating variation in pre-defined gene sets in Yonsei cohort microarray data. The inputs for the GSVA algorithm comprised a gene expression matrix comprising log2 intensity values of patient data. The Gastric cancer patients single cell data was downloaded from Gene Expression Omnibus (GEO; https://www.ncbi.nlm.nih.gov/gds/). ISMARA was used for prediction of shRASD1 regulators using the hg19 reference genome10. The overall contribution of a TF motif was reported as a z-value that represents the average number of standard deviations of the motif activity.

18. Histological and immunohistochemistry analysis

The study was approved by the Institutional Review Board of the College of Medicine at Yonsei University of Korea. We analyzed samples from 31 patients with gastric adenocarcinoma who underwent surgical resection at Severance Hospital, Yonsei University College of Medicine (Seoul, Korea) from 2018. We reviewed all hematoxylin and eosin (H&E) slides used at the time of diagnosis. The IHC staining of RASD1 (1:100, abcam 241924, rabbit polyclonal, Abcam, Cambridge, UK) was performed according to manufacturer’s instructions. All slides were evaluated by experienced pathologist who had no prior knowledge of the selected cases. When discordance in the interpretation occurred, the examiners discussed the results until they reached an agreement.

19. Statistical analysis

Statistical analysis was conducted using a one-way ANOVA test to assess differences among three or more groups, while a student's t-test was used for comparisons between two groups. Statistical significance was denoted as follows: *$p<0.05$, **$p<0.01$, ***$p<0.001$. The data are presented as means with standard error of the mean.

III. RESULTS

1. RASD1, a target gene of GR signaling pathway, is increased in the mesenchymal gastric cancer subtype

To determine whether GR signaling is involved in distinguishing gastric cancer patients subtypes, we analyzed the Yonsei cohort of gastric cancer patients. We conducted a comparison of the GR signaling pathway enrichment score in stem-like subtype, known for its poor prognosis and resistance to chemotherapy, with the Intestinal subtype, which exhibits a contrasting transcriptome profile. Our findings revealed a significant increase in the GR signaling pathway score in the stem-like subtype(n=117) when compared to Intestinal subtype(n=102) (Fig. 1A). Additionally, we examined the target genes of the GR signaling pathway and generated a heatmap for each patient, suggesting a potential association between the GR signaling pathway and aggressiveness of the stem-like subtype in gastric cancer (Fig. 1B). Also, when examining the expression of GR target gene RASD1 and NR3C1 in the Yonsei cohort, both genes were upregulated in the stem-like subtype. (Fig. 1C and 1D).

To further corroborate the role of RASD1 in regulating chemoresistant gastric cancer, we observed RASD1 in a larger cohort of patients with gastric cancer[11]. In this dataset, which included single-cell RNA sequencing of gastric cancer tissue, we focused solely on tumor cells. After applying quality control measures, a total of 7,550 tumor cells were classified into diffuse type (CD44) and intestinal types (EPCAM, MUC13 and COL3A1) based on the expression of previously identified marker genes for each subtype (Fig. 1E). The stem-like subtype displayed similarities with Laurén's diffuse type[5]. This result confirms the increased expressions of NR3C1 and RASD1 in diffuse-type gastric cancer tumors (Fig. 1F). Moreover, we examined the expression of RASD1 in patient tumors of intestinal and diffuse type, respectively (Fig. 1G). While there were variations observed among patients, diffuse-type tumors generally exhibited increased expression of RASD1.

Analyzing the TCGA gastric cancer database, we identified a subgroup of patients with poor survival outcomes, characterized by high RASD1 expression (Fig. 1H). These findings suggest a potential association between high RASD1 expression and poor prognosis in gastric cancer.

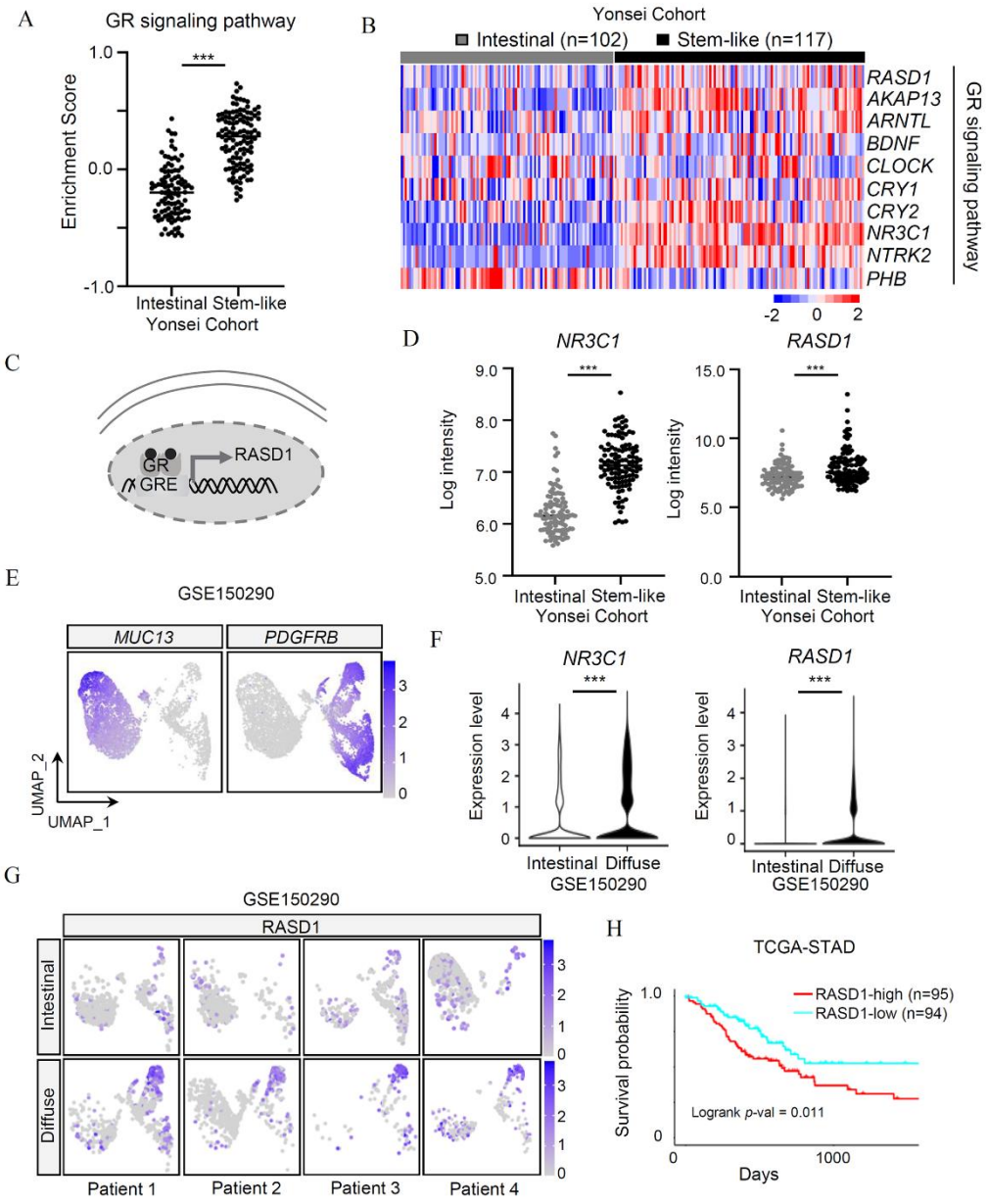

Figure1. RASD1, a target gene of GR signaling pathway, is increased in the mesenchymal gastric cancer subtype. (A) Spearman correlation of intestinal (n=102) and stem-like (n=117) subtype patients GSVA score with expression of GR signaling

pathway. (B) Heatmap depicting the expression of GR signaling pathway target genes in patients from the intestinal (n=102) and stem-like (n=117) subtypes of the Yonsei cohort. (C) A diagram for relation between RASD1 and the GR signaling pathway, indicating that Dexras1 is a target gene of the GR signaling pathway. (D) Comparison of NR3C1 and RASD1 expression levels between different gastric cancer subtypes, specifically intestinal (n=102) and stem-like (n=117). (E) Uniform Manifold Approximation Projection (UMAP) plot of 7,550 tumor cells in gastric cancer tumors. The plot highlights the expression of MUC13 as the intestinal type tumor and PDGFRB as the diffuse type tumor. (F) Violin plots showing the normalized expression of NR3C1 and RASD1 in both intestinal and diffuse type tumor cells in GC tumor. (G) UMAP plot depicting the normalized expression of RASD1 in both intestinal and diffuse type tumors for each patient. (H) Kaplan-Meier plot comparing the RASD1-high group (n=95) and RASD1-low group (n=94) in TCGA-STAD patients, showing a significant Logrank value of 0.011.

2. RASD1 knockdown increases inflammatory response in gastric cancer cell lines

To investigate our findings in vitro, we examined RASD1 expression in GC cell lines (Fig. 2A). We observed a significant upregulation of RASD1 mRNA level in stem-like GC cell lines. Additionally, we utilized transposase-accessible chromatin sequencing (ATAC-seq) and RNA sequencing (RNA-seq) on both intestinal and stem-like cell lines to investigate the differences in each subtype. First, transposase-accessible chromatin was analyzed, showing higher chromatin accessibility in the NR3C1 and RASD1 promoter region of HS746T (a stem-like cell line) compared to NCIN87(an intestinal cell line)(Fig. 2B)[12]. Also, using RNA-seq data we identified that NR3C1 and RASD1 expression was upregulated in stem-like GC cell lines.

To further explore the association of RASD1 with gastric cancer subtype with poor prognosis, we knocked down RASD1 in stem-like subtype gastric cancer cells and examined the transcriptome profile and genomic changes (Fig. 2C). RASD1-knockdown HS746T cells were established, and RNA sequencing was conducted to investigate the molecular mechanisms of RASD1 involvement in the immune system in HS746T cells. The differential expressed genes between shcontrol and shRASD1 showed 1043 gene expression increased and 688 gene expression decreased upon RASD1 knockdown. Notably, genes related to macrophage chemotaxis (CCL3, CCL5, CCL20), macrophage activation (GM-CSF, CXCL1, CXCL2, CXCL3, CXCL5, CXCL8) and TNF receptor superfamily (TNFAIP2, TNFRSF8, TNFRSF9, TNFRSF17, TNFRSF19, TNFRSF13B) target genes exhibited increased expression levels (Fig. 2D and 2E)[13-15].

Pathway enrichment analysis highlighted the enrichment of the TNF-signaling pathway, NF-κB signaling pathway, and cytokine-cytokine receptor interaction pathways when RASD1 expression was knockdown (Fig. 2F). To further investigate the transcription factors affected by RASD1 knockdown, we employed the Integrated System for Motif Activity Response Analysis (ISMARA) algorithm (Fig. 2G). This analysis

confirmed increased activity of the REL-A and IRF transcription factors upon knockdown of RASD1.

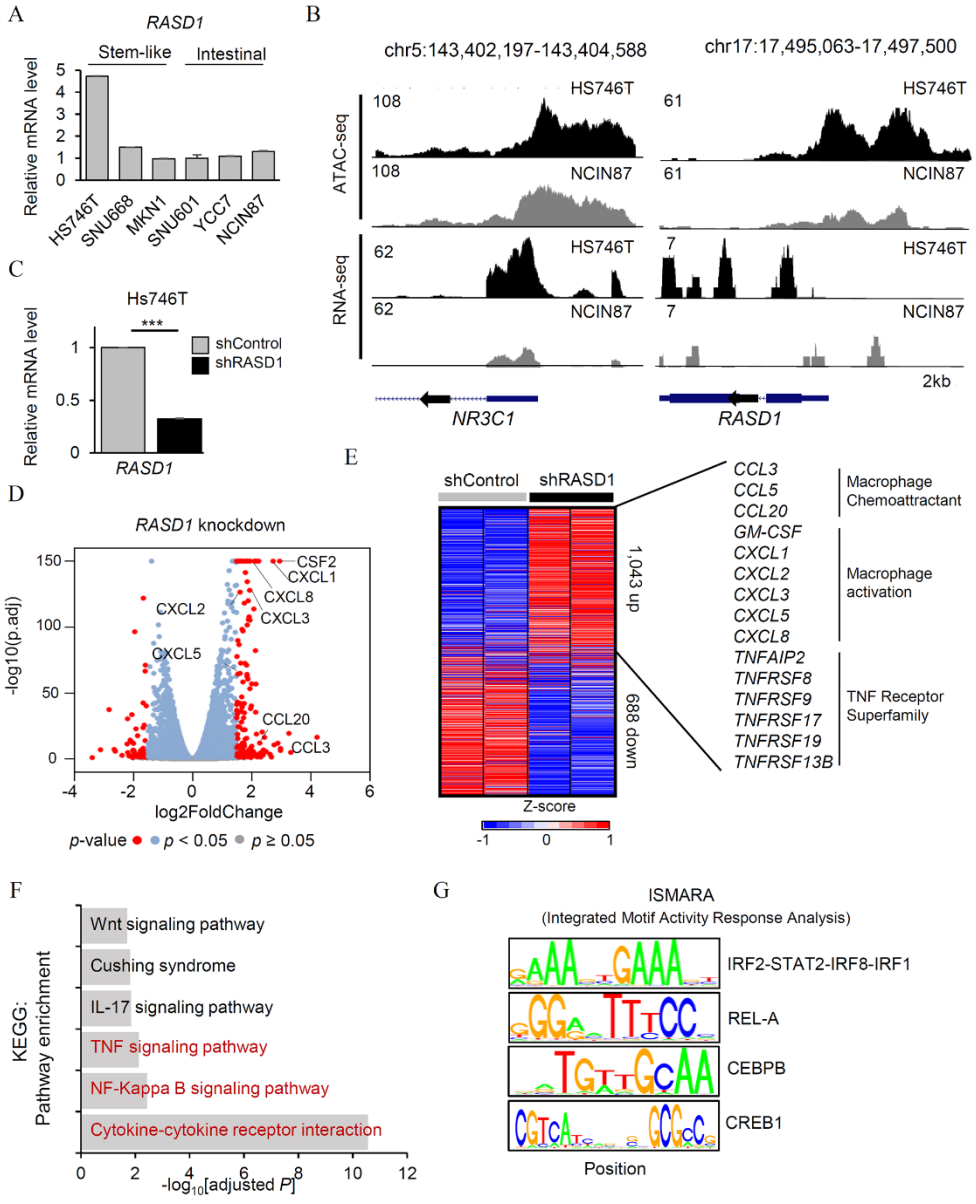

Figure 2. RASD1 knockdown increases inflammatory response in gastric cancer cell lines. (A) Expression levels of RASD1 in gastric cancer cell lines, including stem-like

cells (HS746T, SNU668, MKN1) and intestinal cells (SNU601, YCC7, NCIN87). (B) Representative sequencing tracks for the RASD1 locus, indicating distinct ATAC-seq peaks and RNA-seq peaks at the promoter in gastric cancer cells. The data is normalized for sequencing depth, and the y-axis scale is optimized for peak visualization in each sample. (C) Relative mRNA levels of RASD1 in HS746T cells after knockdown with shRNA. (D) Volcano plots comparing the expression level of DEGs. Each dot represents an expressed gene. Red and blue dots indicate genes significantly upregulated with log2FC≥1. (E) Hierarchical clustering of differentially expressed genes (DEGs) in RASD1 knockdown versus control, based on bulk RNA-seq analysis, showing individual replicates. (F) Top enriched pathways of DEGs resulting from RASD1 knockdown in HS746T cells, analyzed using the KEGG database. (G) ISMARA motif analysis, which is based on z-score, TF-gene Pearson correlation, and average gene target expression change, showing the transcription factor activity changes resulting from RASD1 knockdown in HS746T cells.

3. RASD1 modulates NF-κB signaling via interaction with BRD4

To study RASD1 localization, we conducted immunofluorescence imaging in endogenous HS746T cells. The results revealed that RASD1 is present in both the nucleus and the cytosol, with a predominant localization in the nucleus (Fig. 3A). NF-κB family members are preformed proteins that primarily reside in the cytoplasm, bound to inhibitory proteins of the inhibitor of κB (IκB) family in unstimulated cells. NF-κB plays a critical role in innate inflammation, regulating the expression of inflammatory chemokines[16,17]. Activation occurs through signal-induced phosphorylation and proteasome-mediated degradation of IκB, leading to the release of NF-κB. This allows NF-κB to translocate to the nucleus and initiate transcriptional activation[18]. For nuclear translocation analysis, we transiently transfected RASD1 and analyzed cytoplasmic and nuclear extracts of the cells. We aimed to investigate whether RASD1 directly regulates NF-κB (Fig. 3B). However, RASD1 had no impact on the nuclear import of NF-κB, indicating that RASD1 indirectly regulates the NF-κB signal.

To further validate the transcriptional upregulation of NF-κB expression upon modulation of RASD1, we performed a luciferase assay using the p65 sequence inserted into pGL3-based luciferase reporter plasmids. These plasmids were transfected into 293T cells with RASD1 overexpression, and the luciferase activity of the p65 promoter was measured. Overexpression of RASD1 decreased the luciferase activity of the p65 promoter, confirming its regulatory role in the NF-κB signal (Fig. 3C). NF-κB enhances transcription by interacting with various transcriptional coactivators such as p300, histone deacetylase, and the epigenetic reader protein BRD4[19-21]. As BRD4 is known to enhance the transcriptional activation of NF-κB and belongs to the bromodomain and extraterminal domain (BET) family of transcriptional coactivators[22], we transfected the BRD4 sequence plasmid into 293T cells with RASD1 overexpression. As expected, BRD4 elevated the luciferase activity of p65. However, overexpression of RASD1

reduced the luciferase activity of both p65 and BRD4 (Fig. 3E).

To further investigate the involvement of NF-κB-BRD4 signaling in the inflammatory response, we examined the role of NF-κB/RelA in RASD1-mediated regulation of chemoattractant or cytokine secretion. In our RNA sequencing analysis, we observed increased expression of certain cytokines upon RASD1 knockdown. Among these cytokines, CSF2(GM-CSF) showed the top differential expressed gene, and it is well-known as a target gene for NF-κB[23,24]. CSF2 is a multifunctional cytokine that regulates the inflammatory response. It is mainly produced by various immune cell types, including myeloid cells, dendritic cells, T cells, and B cells[25,26]. Additionally, CSF2 has been found to be produced in tumors[27]. Extensive research has already been conducted on CSF2 as a therapeutic agent for treating tumors[28]. In a previous study, among several proinflammatory cytokines, CSF2 has long-lasting effects, demonstrating its effectiveness in promoting anti-tumor immunity[29].

Based on this knowledge and the fact that CSF2 is a target gene of NF-κB, we hypothesize that CSF2 might play a role in immune modulation by RASD1. To conduct a mechanism study, we performed a reporter assay using the CSF2 luciferase construct (Fig. 3D). We transfected the p65 sequence plasmid into 293T cells with RASD1 overexpression. Surprisingly, overexpression of RASD1 reduced the luciferase activity of p65 and BRD4 (Fig. 3F). While RASD1 regulates the NF-κB signal, NF-κB is not directly regulated by RASD1. Therefore, we subsequently investigate the molecular mechanisms underlying NF-κB and its cofactor, BRD4. We performed a ChIP assay to map the genomic binding of p65 and BRD4 after overexpression of RASD1 (Fig. 3G). Since NF-κB directly induces PD-L1 gene transcription through its promoter binding, we examined the PD-L1 promoter. Notably, BRD4 binding at the PD-L1 promoter was significantly decreased when RASD1 is overexpressed. However, p65 binding between RASD1 overexpression condition remained unchanged. Consistent with this study, we confirmed that RASD1 binds to BRD4, by performing immunoprecipitation assays in

cells transfected with RASD1 alone or co-transfected with BRD4 (Fig. 3H). The result showed that RASD1 indeed interacts with BRD4, indicating that RASD1 primarily influences the binding interaction of BRD4, rather than directly affecting NF-κB. Our findings confirmed that RASD1 inhibits NF-κB-BRD4 binding by scavenging BRD4. Consequently, the interaction between RASD1 and BRD4 leads to an impact on CSF2 promoter transcription. This interaction results inhibition of NF-κB signaling pathway activation, ultimately inducing an anti-inflammatory response within cancer cells (Fig. 3I).

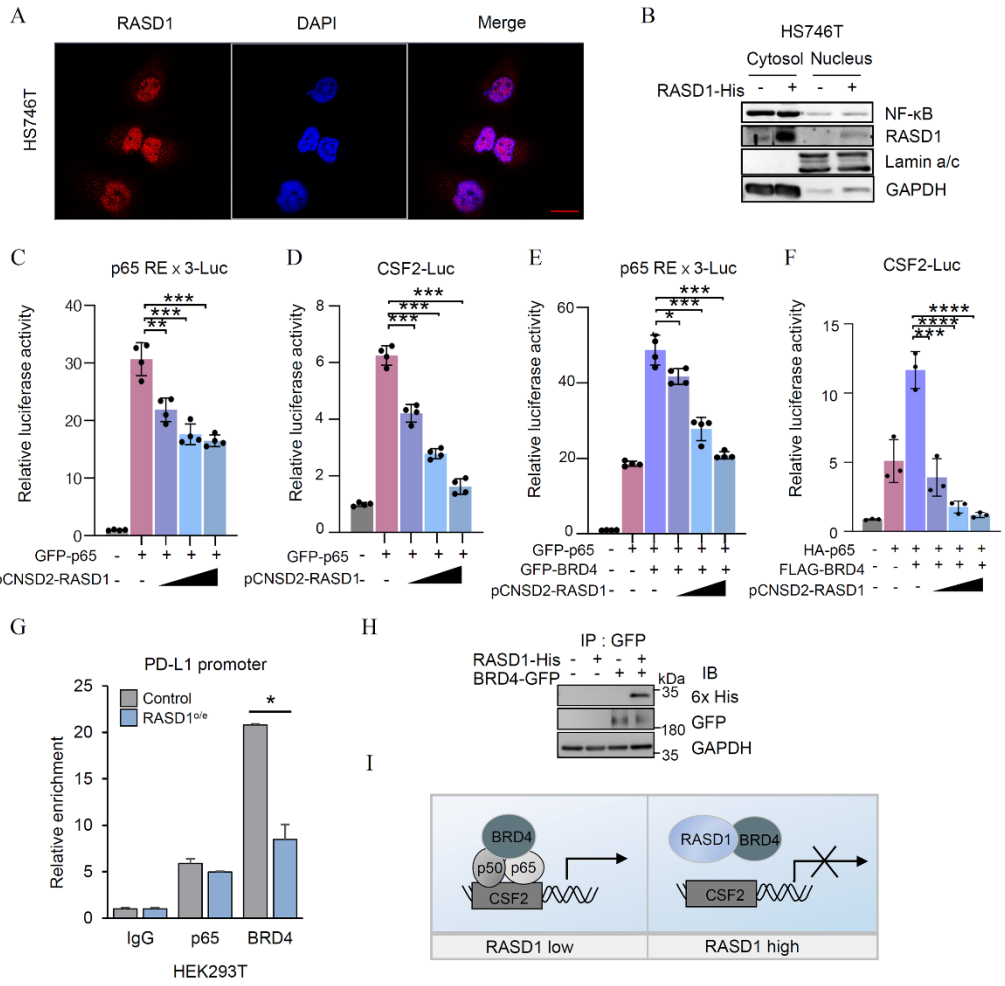

Figure 3. RASD1 modulates NF-κB signaling via interaction with BRD4. (A) Confocal image of HS746T cells stained for RASD1 (in red) and DAPI (in blue). The scale bars represent 20μm. (B) Immunoblot showing the localization of RASD1 in both the nucleus and cytosol of HS746T cells. Lamin A/C was used as a marker for the nuclear fraction, and GAPDH was used as a marker for the cytosolic fraction. (C) GFP-p65 and the p65 Renilla luciferase plasmid were co-transfected into HEK 293T cells with or without RASD1 overexpression. The Renilla luciferase construct was used as a control

for transfection efficiency, and β-gal activity was measured. (D) GFP-p65 and the CSF2 Renilla luciferase plasmid were co-transfected into HEK 293T cells with or without RASD1 overexpression. (E) HEK 293T cells were co-transfected with both GFP-p65 and GFP-BRD4, along with the p65 Renilla luciferase plasmid, either with or without RASD1 overexpression. (F) HEK 293T cells were co-transfected with both HA-p65 and FLAG-BRD4, along with the CSF2 Renilla luciferase plasmid, either with or without RASD1 overexpression. (G) ChIP analysis showed the binding of BRD4 to the promoter of PD-L1 in 293T cells with or without RASD1 overexpression. IgG was used as a negative control. (H) HEK 293T cells were transfected with plasmids encoding His-tagged RASD1 or GFP-tagged BRD4. Cell lysates were subjected to immunoprecipitation with an anti-6X His antibody, anti-GFP antibody and samples were analyzed by Western blotting with antibodies against the 6X-HIS or GFP. Total lysates were also analyzed by Western blotting with the same antibodies. (H) Model scheme depicting how RASD1 scavenges BRD4 to suppress NF-κB-BRD4 binding.

4. In the MC38 syngeneic mouse model, RASD1 overexpression enhances tumor growth and reduces anti-PD1 response

To investigate the role of RASD1 in vivo, we examined the tumor immune response after subcutaneously inoculating MC38 and CT26 mouse carcinoma cell lines into syngeneic mice with intact native immune systems. For this purpose, we generated a cell line overexpressing RASD1 in MC38 cells by transducing vector plasmids containing GFP-RASD1 using a lentivirus delivery system. The stable transfection was confirmed by detecting GFP expression via fluorescence-activated cell sorting (FACS). Additionally, we created a RASD1 knockdown cell line using a shRASD1 vector delivered through lentivirus, followed by puromycin selection to establish RASD1-knockdown MC38 stable cells (Fig. 4A-4D).

First, we evaluated the *in vitro* proliferation rates of MC38 cells with RASD1 overexpression (Fig. 4E). There were no significant differences in proliferation rates between the control and RASD1 overexpressing MC38 cells. To investigate the involvement of the immune system, we further inoculated both RASD1 overexpressing cells and vector control MC38 tumor cells into BALB/c nude mice, which lack cytotoxic T cells (Fig. 4F). However, the results indicated that RASD1 overexpression had no effect on tumor growth in the BALB/c nude mice. Next, we inoculated MC38 tumor cells into syngeneic mice with the same genetic background and transplanted them[30-32]. Surprisingly, when RASD1 overexpressing cells were inoculated into syngeneic mouse hosts, their ability to form tumors significantly increased (Fig. 4G). Our results showed that, their ability to form tumors was significantly increased, suggesting that RASD1 overexpression might have an adverse effect on tumor immune system. Next, we examined the in vitro proliferation assay and tumor growth effects of RASD1-knockdown MC38 cells in both BALB/c nude mice and immunocompetent C57BL/6J mice (Fig. 4H-4J). However, the results did not show any significant antitumor immune response upon reducing RASD1 expression in MC38 cells.

Next, we sought to validate the responsiveness to anti-PD1 therapy using MC38 tumor-bearing mice (Fig. 4K). After injecting MC38-control and MC38-RASD1 overexpressed cells into mice, we treated with anti-PD1 or an isotype control, and then analyzed the tumor growth (Fig. 4L). The anti-PD1 treatment significantly reduced MC38-control tumor growth. However, RASD1 overexpressed MC38 tumor showed resistance in anti-PD1 therapy. Additionally, compared with MC38-control tumor, the RASD1 overexpressed MC38 tumor showed significantly increased tumor growth. These data suggest that RASD1 expression reduces the responsiveness to anti-PD1 therapy.

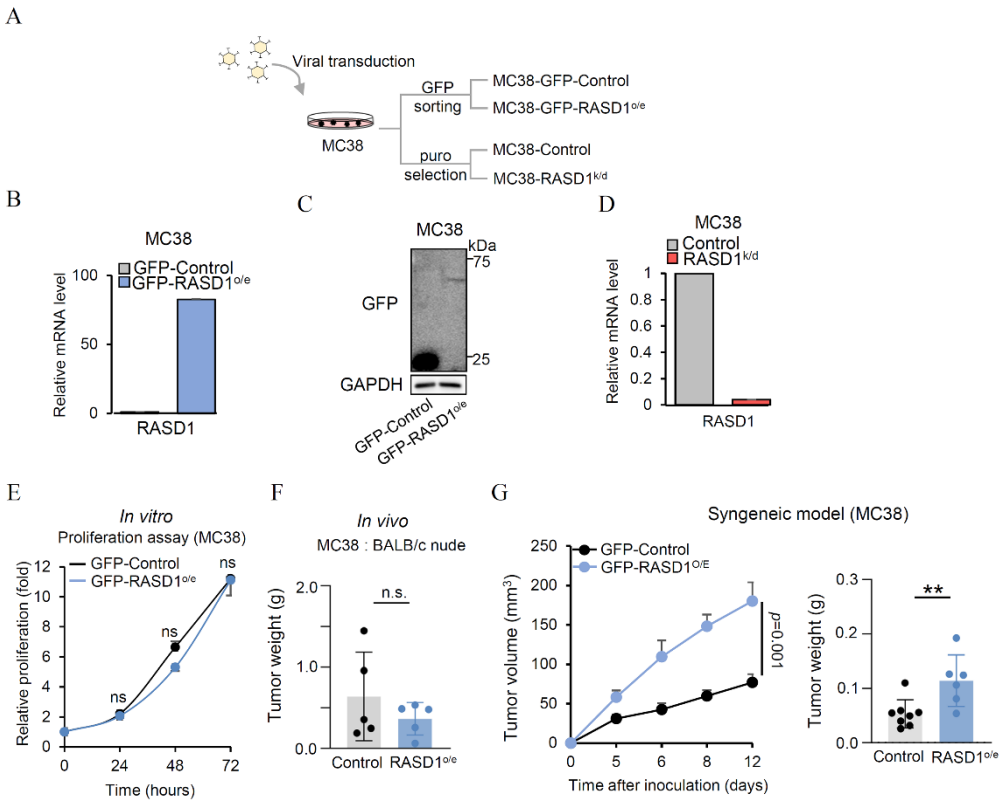

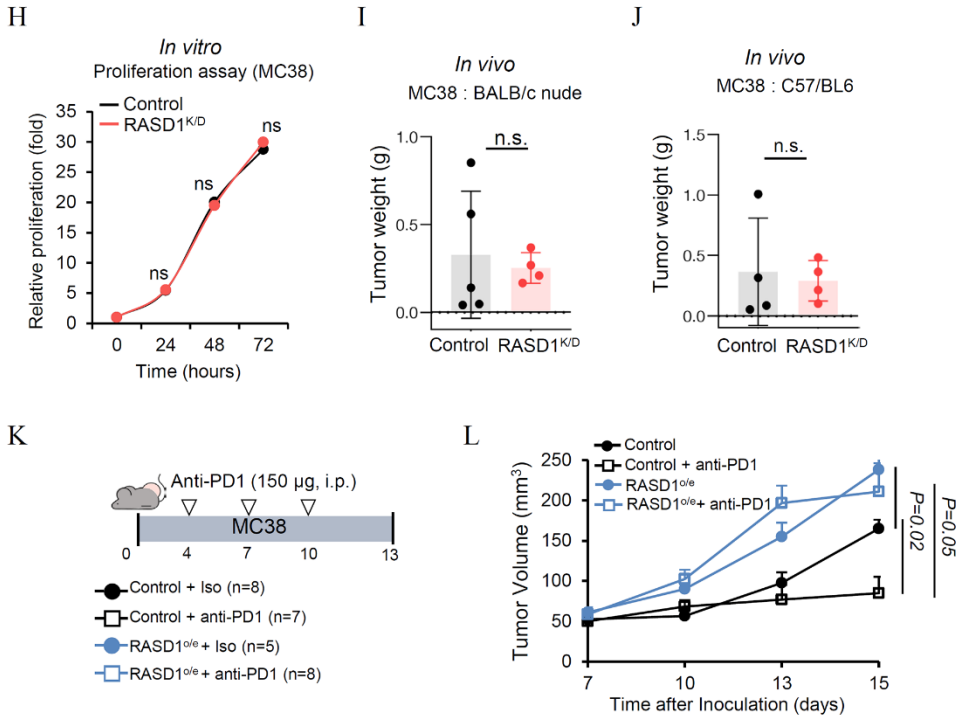

Figure 4. In the MC38 syngeneic mouse model, RASD1 overexpression enhances tumor growth and reduces anti-PD1 response. (A) Schematic diagram of MC38 cells transduced with lentivirus. MC38 cell line was transduced with either GFP control lentivirus or lentivirus containing GFP-RASD1. RASD1 knockdown MC38 cell line was transduced with shRASD1 lentivirus. (B) Relative mRNA levels of RASD1 in MC38 cells after overexpression. The expression levels were quantified and normalized to the control group. (C) Western blot analysis showing the expression of GFP-RASD1 in MC38 cell lines. GAPDH was used as a loading control. The analysis was performed twice with biologically independent samples. (D) Relative mRNA levels of RASD1 in MC38 cells after knockdown. The expression levels were quantified and normalized to the control group. (E) In vitro proliferation assay of MC38-GFP-control and MC38-GFP-RASD1 cell lines. Cells were counted using the CCK-8 method. Three

independent experiments were performed for each group. (n=3/group) (F and G) Endpoint tumor weight of vector control and RASD1 overexpressed MC38 tumors. Approximately 2 x 10^5 tumor cells were injected subcutaneously into BALB/c nude mice (F), and into C57BL/6 mice (G) Error bars show means ±s.e.m. P-values were calculated using two-way ANOVA. (H) In vitro proliferation assay of MC38-shcontrol and MC38-shRASD1 cell lines. Cells were counted using the CCK-8 method. Three independent experiments were performed for each group. (n=3/group) (I and J) Endpoint tumor weight of vector shcontrol and shRASD1 in MC38 tumors. Approximately 2 x 10^5 tumor cells were injected subcutaneously into BALB/c nude mice (I), and into C57BL/6 mice (J) Error bars represent means ±s.e.m. P-values were calculated using two-way ANOVA. (K) Treatment schedule for RASD1 overexpressed MC38 cells in C57BL/6 mice. Mice were implanted subcutaneously with RASD1 overexpressed MC38 cells and subsequently treated with an anti-PD1 antibody at the indicated times. Tumor formation was monitored and analyzed during the observation period. (L) Tumor-growth delay in mice bearing RASD1 overexpressed MC38 tumors with or without anti-PD1 treatment. Error bars show means ±s.e.m. P-values were calculated using two-way ANOVA.

5. In the CT26 syngeneic mouse model, RASD1 knockdown enhances responsiveness to anti-PD1 response

Next, to confirm the differential efficacy of PD-1 blockade, we utilized CT26 cancer cells, which are known to be less sensitive to anti-PD1 therapy. Firstly, we generated cell lines with both overexpressed and knocked down RASD1 expression in CT26 cells (Fig. 5A-5C). The lentivirus delivery system was used to transduce GFP-RASD1 vector plasmids, and FACS was performed to create RASD1 overexpressed CT26 cells. Additionally, we created RASD1 knockdown CT26 cells using the shRASD1 vector, and puromycin selection was performed to generate RASD1 knockdown CT26 cells.

Like MC38 tumors, RASD1 overexpressed and knocked down CT26 cells showed no significant proliferation rates (Fig. 5D). Additionally, there was no effect on tumor growth in BALB/c nude mice (Fig. 5E). Next, we examined tumor growth when RASD1 was overexpressed in CT26 cells in a syngeneic mouse model (Fig. 5F). However, in CT26 cells, overexpression of RASD1 did not increase tumor growth.

Next, we conducted the same experiments with the RASD1 knockdown CT26 cell line. There was no difference in cell proliferation in vitro, and tumor weight in BALB/c nude mice showed no significance changes (Fig. 5G and 5H). However, in the case of CT26 RASD1 knockdown cells, the tumor weight was reduced (Fig. 5I). We hypothesized that these changes were due to the difference in RASD1 expression levels in each cell line (Fig. 5J). In the case of the MC38 cell line, the mRNA level of RASD1 was low, so overexpression of RASD1 resulted in an increase in tumor size. In the case of the CT26 cell line, RASD1 mRNA levels were high, so knockdown of RASD1 expression resulted in a decrease in tumor size.

Subsequently, we analyzed the anti-PD1 efficacy in RASD1 knockdown CT26 cells (Fig. 5K). Importantly, RASD1 knockdown CT26 tumors seemed to be responsive to anti-PD1 therapy (Fig. 5L). Additionally, RASD1 knockdown CT26 tumors showed

reduced tumor size and cleared tumors compared to the control. These results confirmed that responsiveness to anti-PD1 therapy increased upon RASD1 knockdown. Through these *in vivo* experiments, we further established that RASD1 is a gene that regulates immune suppression. Based on these results, we hypothesized that RASD1 plays a role in inhibiting immune cell infiltration and promoting a pro-tumorigenic response. These findings provide effective strategies for overcoming resistance to anti-PD1 therapy. Based on these results, we dissociated and flow-sorted RASD1 overexpressed tumors and control tumors, isolating $CD45^+$ immune cells and $CD45^-$ non-immune cells, which were subjected to single-cell RNA sequencing.

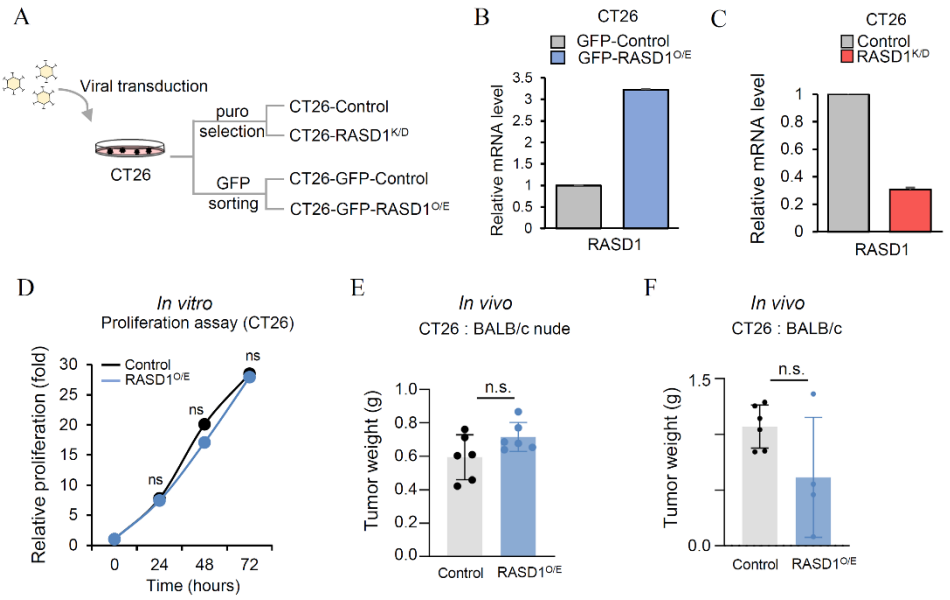

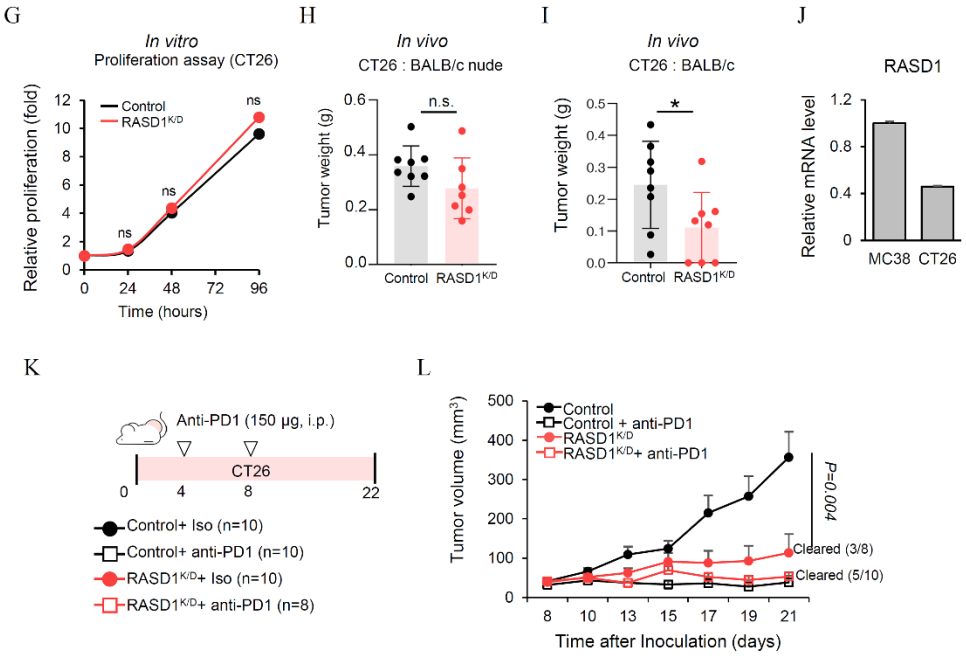

Figure 5. In the CT26 syngeneic mouse model, RASD1 knockdown enhances responsiveness to anti-PD1 response. (A) Schematic diagram of CT26 cells transduced with lentivirus. CT26 cell line was transduced with either GFP control lentivirus or lentivirus containing GFP-RASD1. RASD1 knockdown CT26 cell line was transduced with shRASD1 lentivirus. (B) Relative mRNA levels of RASD1 in CT26 cells after overexpression. The expression levels were quantified and normalized to the control group. (C) Relative mRNA levels of RASD1 in CT26 cells after knockdown. The expression levels were quantified and normalized to the control group. (D) In vitro proliferation assay of CT26-GFP-control and CT26-GFP-RASD1 cell lines. Cells were counted using the CCK-8 method. Three independent experiments were performed for each group. (n=3/group) (E and F) Endpoint tumor weight of vector control and RASD1 overexpressed CT26 tumors. Approximately 2×10^5 tumor cells were injected subcutaneously into BALB/c nude mice (E), and into BALB/c mice (F). Error bars show means ±s.e.m. P-values were calculated using two-way ANOVA. (G) In vitro

proliferation assay of CT26-shcontrol and CT26-shRASD1 cell lines. Cells were counted using the CCK-8 method. Three independent experiments were performed for each group. (n=3/group) (H and I) Endpoint tumor weight of vector shcontrol and shRASD1 in CT26 tumors. Approximately 2×10^5 tumor cells were injected subcutaneously into BALB/c nude mice (H), and into BALB/c mice (I). Error bars represent means ±s.e.m. P-values were calculated using two-way ANOVA. (J) Real-time PCR results showing the relative expression levels of RASD1 in MC38 and CT26 cell lines. The data are presented as mean ± standard error of the mean (SEM) from three independent experiments. The expression levels were normalized to the reference gene 36B4 for each sample. (K) Treatment schedule for RASD1 knockdown CT26 cells in BALB/c mice. Mice were implanted subcutaneously with RASD1 knockdown CT26 cells and subsequently treated with an anti-PD1 antibody at the indicated times. Tumor formation was monitored and analyzed during the observation period. (L) Tumor-growth delay in mice bearing RASD1 knockdown CT26 tumors with or without anti-PD1 treatment. Error bars show means ±s.e.m. P-values were calculated using two-way ANOVA.

6. Changes in infiltrating immune cells examined in tumors derived from RASD1-overexpressing cancer cells

The transcriptomes of individual cells were analyzed through scRNA-seq using the 10x Genomics platform (Fig. 6A). Subsequently, we verified that RASD1 expression was increased in $CD45^{-}GFP^{+}$ cells, and it was confirmed that the mRNA level of CSF2, a cytokine regulated by RASD1, was decreased (Fig. 6B). Immunohistochemistry was conducted to examine CD45 expression in tumors (Fig. 6C). After filtering out low-quality cells, removing doublet reads, and correcting for batch effects, the transcriptomes of a total of 23,866 high-quality single cells were analyzed.

Analysis was performed on 11,746 single cells obtained from MC38 control tumor-infiltrating immune cells and 12,120 single cells obtained from MC38-RASD1 overexpressed tumor-infiltrating immune cells. Uniform Manifold Approximation and Projection (UMAP) dimensionality reduction of the transcriptomes revealed distinct clusters of cells present in immune cells from control and RASD1 overexpressed tumors (Fig. 6D and 6G). We used Seurat to analyze the gene expression differences among the cell clusters and identify the genes that were upregulated in different cells. Finally, the distribution of 8 different cell clusters was determined based on unbiased cell type recognition (Fig. 6E and 6F). These cell clusters were named according to specific marker genes: Macrophages (expressing Apoe, Mrc1), Monocytes (expressing Ly6c2, Plac8), MDSC (expressing S100a9, Cxcl2), T cells (expressing Cd3d, Cd8a), NK cells (expressing Nkg7, Xcl1), cDC (expressing Fscn1, Socs2), pDC (expressing Siglech, Ly6d), and B cells (expressing Cd79a, Cd79b). To further understand the cell clustering, we compared immune cells from control tumor and RASD1 overexpressed tumors by grouping, and their cell proportions were also analyzed (Fig. 6H). Following RASD1 overexpressed tumor, the proportion of monocyte populations was increased whereas the macrophage populations were decreased.

Moreover, analyzing cell type-specific transcriptional signatures helps gain insights into intercellular interactions mediated by secreted and membrane-bound proteins. To map intercellular crosstalk in RASD1-mediated immune cell interactions, we utilized the CellChat algorithm[33]. This algorithm employs a database of interactions among ligands, receptors, and their cofactors to infer potential communications between cell types in scRNA-seq data. Through a heatmap visualization, we displayed the differential number of interactions in immune cells from control and RASD1 overexpressed tumors (Fig. 6I). Additionally, we compared the outgoing and incoming interaction strengths to identify cell populations with significant changes in the immune cells from control and RASD1 overexpressed tumor datasets (Fig. 6J). This analysis highlighted prominent differences in potential interactions between monocytes and macrophages. Therefore, we focused on analyzing the changes specifically related to monocytes and macrophages.

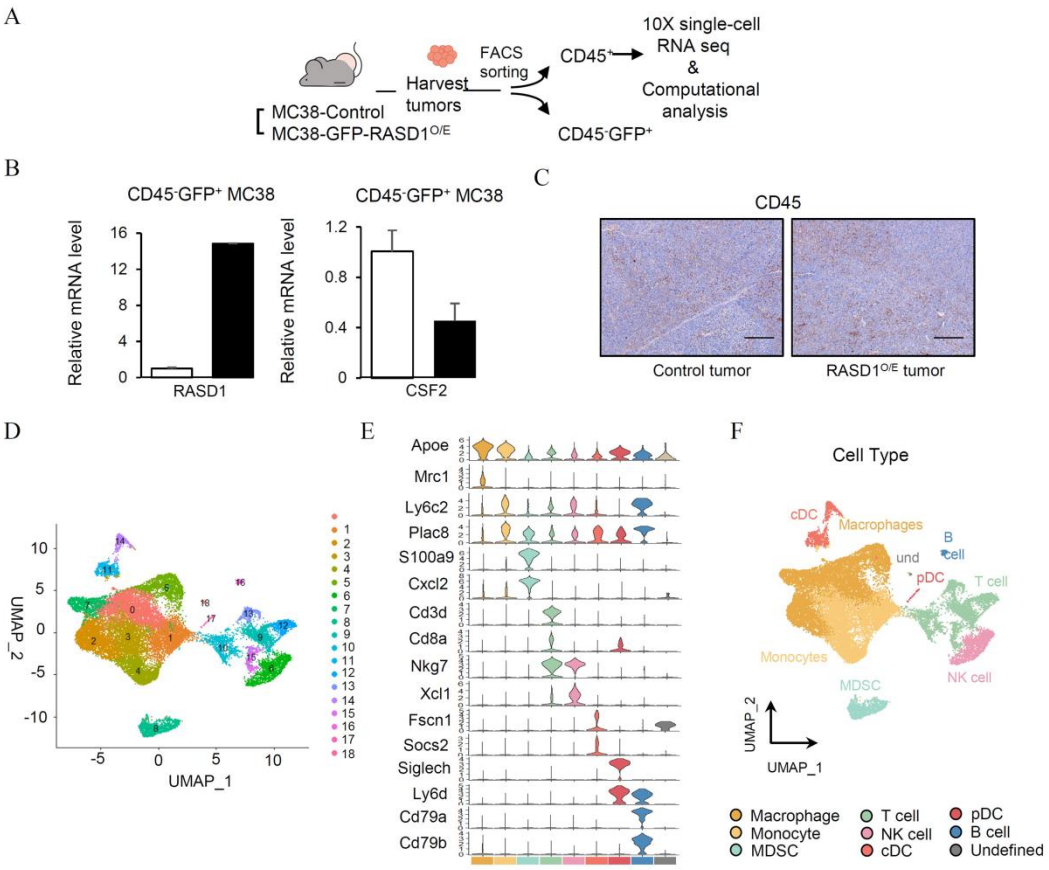

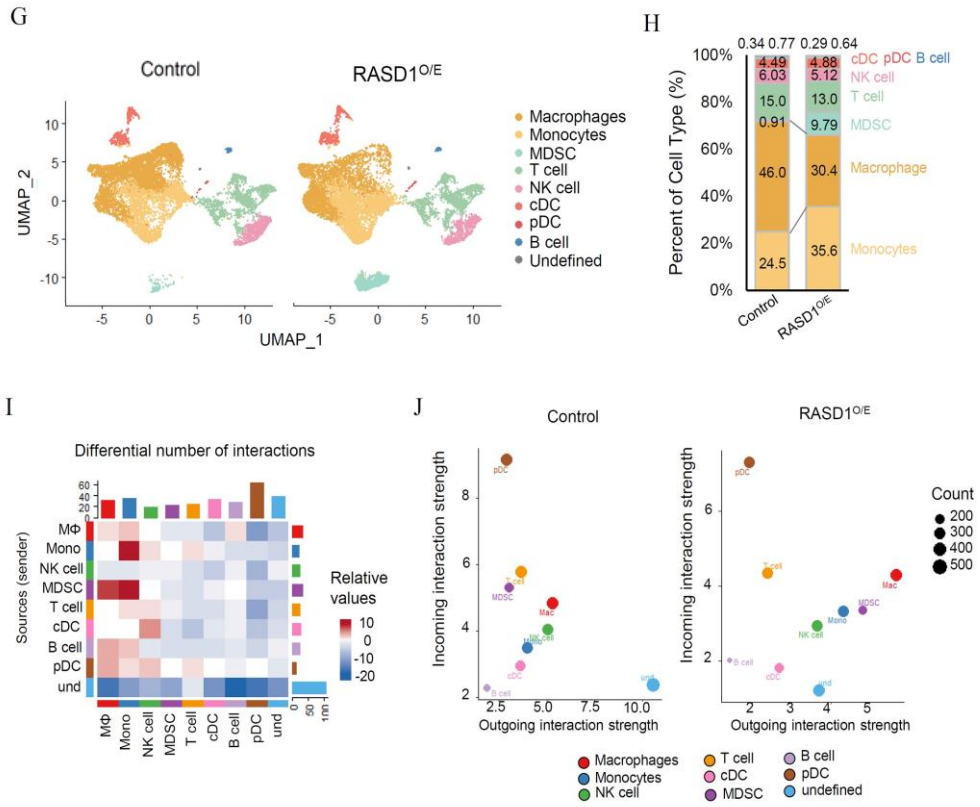

Figure 6. Changes in infiltrating immune cells examined in tumors derived from RASD1-overexpressing cancer cells. (A) Experimental design and analysis of single cells from MC38-control and MC38-RASD1 overexpressed tumor samples. (B) Relative mRNA level in $CD45^{-}GFP^{+}$MC38 cancer cells. The left panel shows the quantification of RASD1 mRNA expression, and the right panel shows the relative mRNA level of CSF2, a cytokine regulated by RASD1. (C) Representative images of immunohistochemistry (IHC) staining with CD45 in control and RASD1 overexpressed tumor samples in MC38. Scale bar, 200μm. (D) UMAP visualization of tumor infiltrating immune cells, where

each cell is colored based on the clustering results obtained through single-cell RNA sequencing. (E) Violin plots showing the expression levels of known marker genes in each cell cluster. (F) UMAP plot depicting the major cell types identified through single-cell RNA sequencing of tumor infiltrating lymphocytes (TILs). (G) UMAP visualization of cells after integration. (H) Bar chart of the relative percentage of immune cells in the control group and RASD1 overexpressed group, respectively. (I) Heatmap displaying the differential numbers of interactions between control and RASD1 overexpressed tumor infiltrating immune cells. In the color bar, red indicates increased signaling in the second dataset compared to the first, while blue indicates decreased signaling. (J) Scatter plot depicting the senders (sources) and receivers (targets) of intercellular communications for each dataset. The positions of the data points indicate the strength and direction of the interactions, with specific cell populations labeled as senders or receivers.

7. Expression level of RASD1 in cancer cells influences the ratio of macrophage over monocyte inside the tumor

To better understand and more accurately define the monocyte/macrophage clusters identified by single cell RNA-seq, we computationally separated monocyte/macrophage cells and reanalyzed the data. Monocytes are produced in the bone marrow and give rise to $LY6C^{+}$ classical monocytes, which are recruited to sites of infection, tissue injury, and tumors, while $LY6C^{-}$ non-classical monocytes detect pathogens and maintain vessel integrity. Sub-clustering analysis of 4500 monocytes identified 5 subclusters, all of which are $LY6C^{+}$ monocytes (Fig. 7A and 7B). The annotation of these subclusters was based on published monocyte marker genes (Fig. 7C). Two subclusters, "MHC II-Mono" and "C1q-Mono," showed changes in monocytes from RASD1 overexpressed tumor (Fig. 7D). RASD1 overexpressed tumor infiltrating monocytes resulted in reduced monocyte differentiation into macrophages, prompting a focus on the differentiation and expansion of monocyte lineages. The Ccr2-Ccl2 axis plays a key role in regulating the recruitment and retention of monocytes to metastatic sites[34,35]. Additionally, monocytes migrate to tumor locations in a manner dependent on Ccr2, and once there, they differentiate into macrophages, promoting cancer growth[36]. Consequently, Ccr2 expression was decreased in RASD1 overexpressed tumor infiltrating monocytes (Fig. 7E).

Next, we analyzed macrophage cells through sub-clustering. In the tumor microenvironment, tumor-associated macrophages (TAMs) adopt a different role and promote cancer cell growth, metastasis, and immunosuppression on adaptive immune cells[37,38]. TAMs constitute the most abundant immune population within the tumor microenvironment and display a wide range of properties, ranging from anti-tumorigenic to pro-tumorigenic[39]. Antitumorigenic TAMs retain characteristics of antigen-presenting cells (APCs), such as high expression of MHCⅡ, phagocytic capability, and the ability to kill tumor cells[40]. On the other hand, pro-tumorigenic TAMs exhibit immunosuppressive properties, with low expression of MHCII and the presence of inhibitory molecules[41].

To investigate the heterogeneity and role of macrophages from RASD1 overexpressed tumor TILs, we performed an unsupervised cluster analysis (Fig. 7F). Five macrophage subclusters were identified: Spp1 mΦ, characterized by the expression of Spp1, Arg1, and Mmp12, known to have immunosuppressive properties; MHCII Mϕ, expressing relatively high levels of antigen-presentation genes (H2-Aa, H2-Eb1); Ribosomal mΦ, enriched in Rps2, Rps18 and Rpl14 genes; M2 Mϕ, identified by the expression of Retnla, Mrc1, and Ccl18, confirmed as markers of anti-inflammatory functions; and Proliferative mΦ, expressing high levels of proliferative genes (Mki67, Top2a, Ube2c), which were confirmed to be associated with proliferation and growth of tumors (Fig. 7G). Only one subcluster, Spp1-MΦ was dominant in RASD1 overexpressed TAMs (Fig. 7H). Spp1-MΦ was known to exhibit immunosuppressive properties and is positively correlated with tumorigenesis and metastasis[42]. To further identify Spp1-MΦ, we compared Spp1-MΦ increased DEGs and decreased DEGs (Fig. 7I). We detected 651 up-regulated DEGs and 1265 down-regulated DEGs. Spp1-MΦ from RASD1 overexpressed tumor expressed genes involved in angiogenesis, such as Vegfa, and immunosuppression, such as Spp1, CD274, and Arg1(Fig. 7J).

Moreover, suppressing inflammation signaling induced by cytokines produced in TME like CSF2 and IL-1β can reduce monocyte recruitment and TAM accumulation in tumors. We aimed to examine the expression of CSF2 receptor in immune cells, which was reduced in tumor cells upon RASD1 overexpression (Fig. 7K). The expression of CSF2RA in tumor associated macrophages resulted in reduced expression in RASD1 overexpressed TAMs.

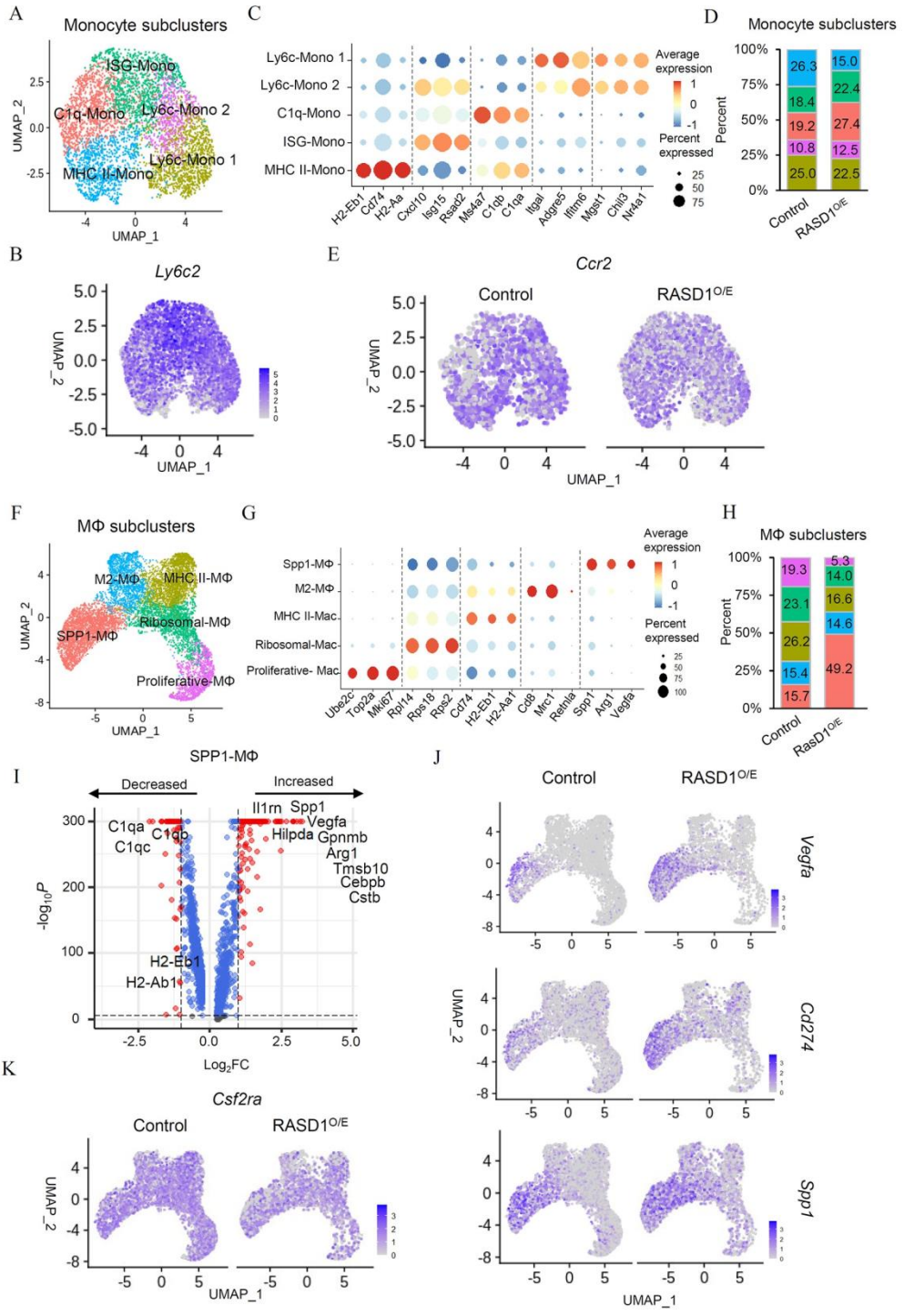

Figure 7. Expression level of RASD1 in cancer cells influences the ratio of macrophage over monocyte inside the tumor. (A) UMAP plot of monocytes subclusters. (B) Feature plot displaying the expression level of Ly6c2 in each monocyte cluster. (C) Dot plot of representing the expression of representative marker genes for each monocyte cell subset. The color scale indicates the average marker gene expression, while the dot size represents the percentage of cells expressing the marker gene. (D) Bar plot showing the relative percentage of monocyte subclusters in the control tumor group and the RASD1 overexpressed tumor group, respectively. (E) Feature plot showing the expression of the monocyte differentiation marker gene Ccr2. (F) UMAP plot depicting 9278 macrophages (MΦ) from the tumor infiltrating lymphocytes, color-coded to represent different subclusters. (G) Dot plot of representing the expression of representative marker genes for each MΦ cell subset. The color scale indicates the average marker gene expression, while the dot size represents the percentage of cells expressing the marker gene. (H) Bar plot showing the relative percentage of macrophage subclusters in the control tumor group and the RASD1 overexpressed tumor group, respectively. (I) Volcano plots representing gene sets of increased and decreased expression in the Spp1- MΦ cluster. The plots display log2FC on the x-axis and adjusted P-values on the y-axis. The default cut-off for log2FC is >|2|; the default cut-off for P value is $10e^{-6}$. (J) Feature plot displaying the expression level of genes associated with immune suppression in TAMs from control tumor and RASD1 overexpressed tumor. The plot shows the distribution of gene expression levels in the two groups. (K) Feature plot showing the expression of the receptor for the marker gene CSF2, which induces macrophage differentiation, in TAMs from control tumor and RASD1 overexpressed tumors.

8. Recombinant CSF2 treatment activates macrophages in tumors validation RASD1 expression as an immunotherapy biomarker

Since it was confirmed that tumors in which RASD1 expression is increased exhibited immune suppressive characteristics, we then elucidate the effects of RASD1 inhibition. To target RASD1-overexpressing tumors, we attempted therapy using recombinant CSF2. In a syngeneic mouse model with RASD1 overexpressed MC38 cells, we initiated treatment with recombinant CSF2 and anti-PD1 injections on day7 to monitor tumor growth (Fig. 8A). CSF2 was administered once every 7 days, and anti-PD1 was administered three times at 3-day intervals starting from day11. Treatment of mice bearing RASD1 overexpressed tumors with recombinant CSF2 or anti-PD1 treatment alone had a smaller effect on decreasing tumor growth. However, the combination of recombinant CSF2 and PD1 blockade significantly reduced tumor growth (Fig. 8B). We further quantified M1 and M2 macrophages in RASD1 overexpressed MC38 tumors using flow cytometry after drug administration (Fig. 8C). The analysis revealed a significant increase in the number of M1 macrophage markers in the combination treatment group, while the M2 macrophage phenotype was significantly reduced (Fig. 8D). However, there were no significant increases in the number of $CD8^+$ T cells. Additionally, we investigated the possibility of treating RASD1-overexpressed tumors with CSF2 (Fig. 8E). Using MC38 control and MC38-RASD1 overexpressed cell lines, we inoculated these cell lines into syngeneic mouse. Then, we examined whether RASD1-overexpressed tumors are regulated by CSF2. Consistent with previous results, RASD1-overexpressed tumors increased compared to the control group. Also, we confirmed that injecting CSF2 into the RASD1-overexpressed tumor significantly reduced tumor growth. These findings prompted us to assess the RASD1-overexpressed tumors were suppressed in CSF2 dependence.

To validate RASD1 as a prognostic biomarker, we used tumors from 31 patients with GC who received immune checkpoint blockade therapy (Fig. 8E). Among the 31 patients,

CR (Complete Response) and PR (Partial Response) each accounted for 3.25%, SD (Stable Disease) accounted for 35.4%, and PD (Progressive Disease) accounted for 58%. RASD1 expression was checked in the tissues of these patients (Fig. 8F). The representative IHC staining of RASD1 is shown in Fig. 8G. Immunohistochemistry staining showed that RASD1 was highly expressed in ICB non-responder GC tissues. Additionally, when examining gastric cancer tissues from all 31 patients, RASD1 expression was increased in the ICB non-responder group (Fig. 8H). Furthermore, we obtained data from previously published cohorts[43]. Among the 26-patient cohort with advanced gastric cancer treated with ICI, an increased in RASD1 expression was observed in the non-responder group (Fig. 8I). Tumors in the ICI non-responsive group SD, PD showed enrichment for high RASD1 expression. These patients' tumors were analyzed using bulk RNA sequencing, and the patients were stratified based on RASD1 expression levels.

Using analytical tools with xCell, we accurately estimated the abundance of macrophages and $CD8^+$ T cells through deconvolution of patient ICB bulk RNA-sequencing data to determine the immune scores (Fig. 8J). In the responder group, we observed higher proportions of M0 macrophages and M1 macrophages. However, there was no difference in the proportions of naïve $CD8^+$ T cells, cytotoxic T cells, and regulatory T cells between the responder and non-responder groups. Interestingly, in the non-responder group, high RASD1 expression is associated with a lack of M1 macrophage morphology, which is typically associated with inflammation and better outcomes. These findings from gastric cancer patients undergoing immunotherapy suggest that RASD1 overexpression in tumors may lead to an immunosuppressive tumor microenvironment and reduced immunotherapy response.

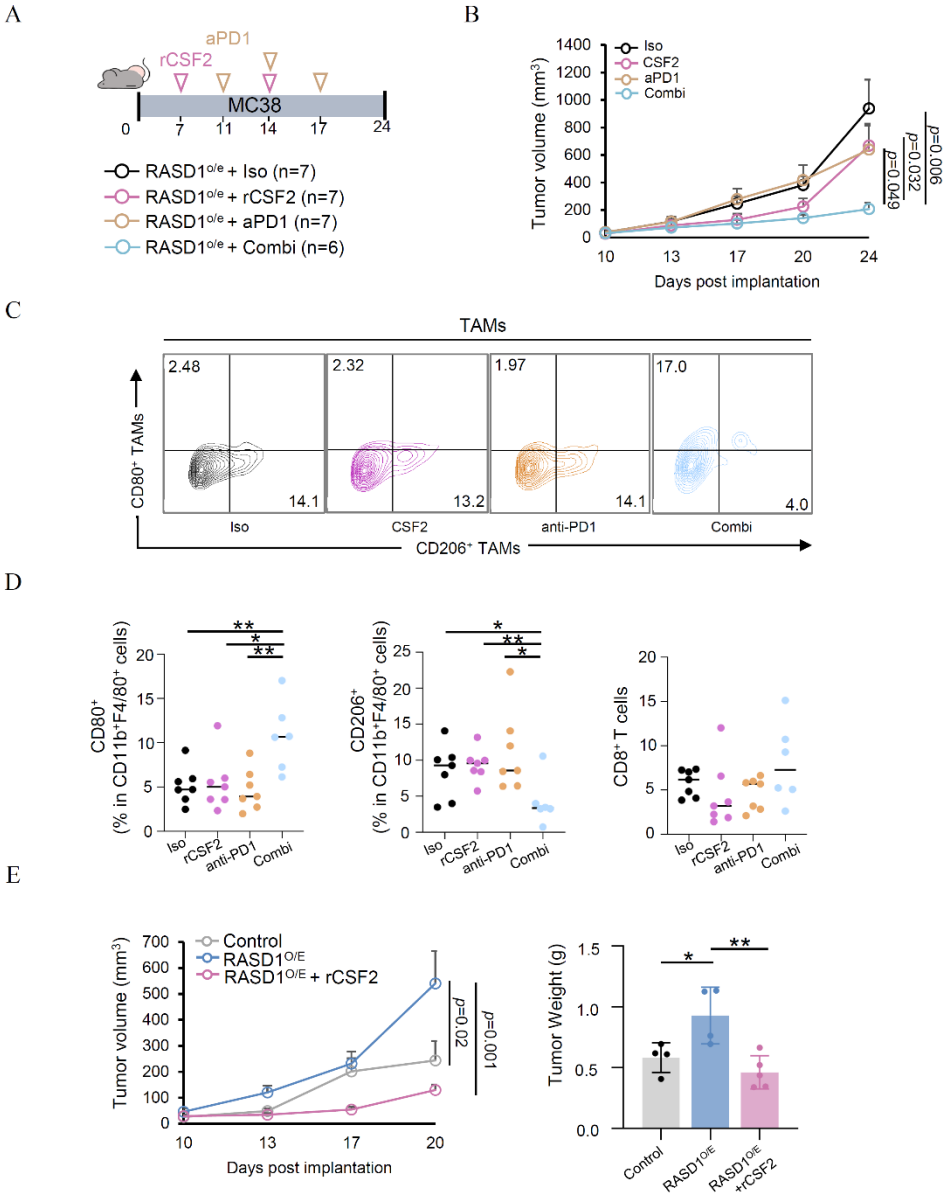

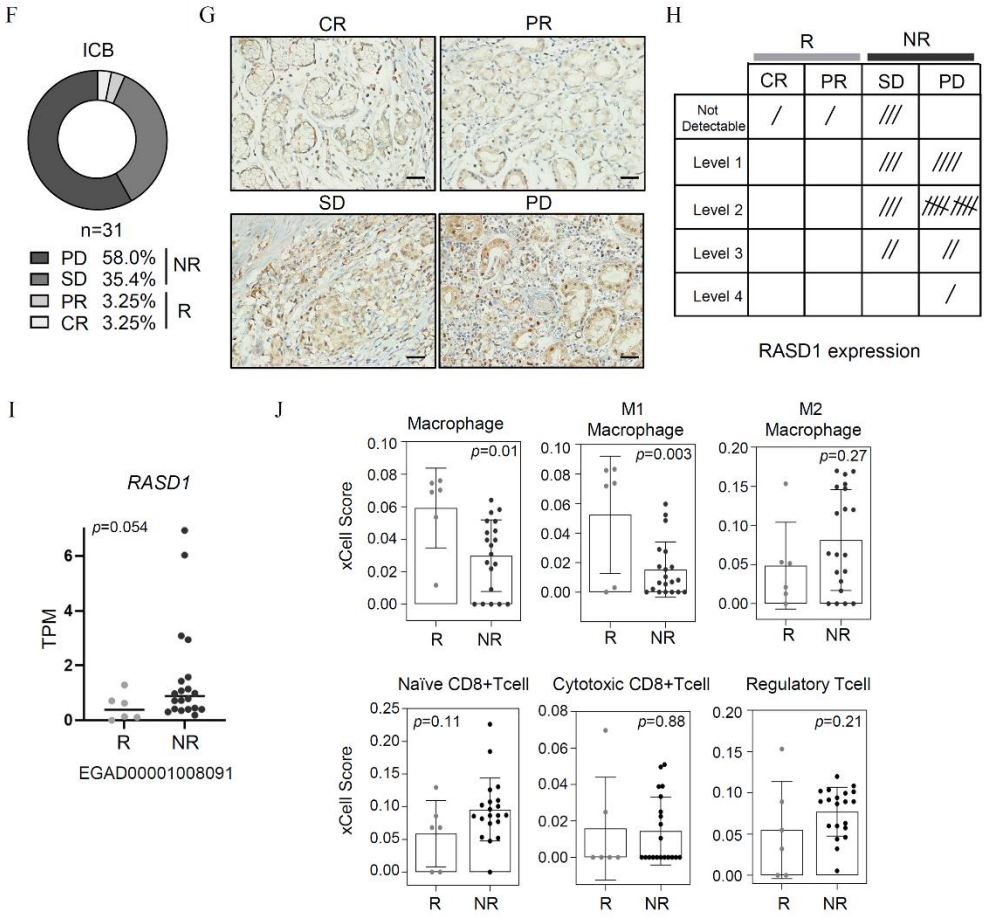

Figure 8. recombinant CSF2 treatment activates macrophages in tumors and validation RASD1 expression as an immunotherapy biomarker. (A) Treatment schedule for RASD1 overexpressed MC38 cells in C57/BL6 mice. Mice were implanted subcutaneously with RASD1 overexpressed MC38 cells and subsequently treated with a recombinant CSF2 and anti-PD1 at the indicated times. Tumor formation was monitored and analyzed during the observation period. (B) Tumor-growth delay in mice bearing RASD1 overexpressed MC38 tumors with recombinant CSF2 and anti-PD1 treatment. Error bars show means ±s.e.m. P-values were calculated using two-way ANOVA. (C, D)

Measure macrophage proportions using flow cytometry, (E) Endpoint tumor weight of vector control and RASD1 overexpressed MC38 tumors. Approximately 2×10^5 tumor cells were injected subcutaneously into C57BL/6 mice. 5μg of recombinant CSF2 was i.p injected, or vehicle control. Error bars represent means ±s.e.m. P-values were calculated using two-way ANOVA. (F) Response pattern of GC patients who received ICB therapy (*n*=31) at Severance Hospital. (G) RASD1 staining in human gastric cancer tumor tissue. Magnification, 40× objective. Scale bars are equivalent to 100μm. (H) Statistical analysis of immunohistochemistry results of RASD1 expression in 31 human GC patients who received immune checkpoint blockade therapy; CR: Complete Response, PR: Partial response, SD: Stable Disease, PD: Progressive Disease. (I) Expression of RASD1 stratified based on responders (CR/PR) and non-responders (SD/PD) This analysis involved 28 patients treated with anti-PD1 at Seoul St. Mary's hospital. (J) Using analytical tools xCell, estimated the abundance of macrophages and $CD8^+$ T cells through deconvolution of patient ICB bulk RNA-sequencing data to determine the immune scores.

IV. DISCUSSION

Collectively, our findings elucidate that GR, which has anti-inflammatory and immune-suppressive characteristics, is associated with chemo-resistant gastric cancer. More specifically, we show that RASD1, a target gene of GR, has high expression in incurable gastric cancer and induces antitumor immunity. We uncovered that RASD1 regulates NF-κB signaling through interaction with BRD4 and found that RASD1 ablation promotes patients with high expression of RASD1. Finally, we uncovered a potential prognostic biomarker of RASD1 in gastric cancer patients treated with immune checkpoint inhibitors.

Our findings indicate that GR induces RASD1 expression and inhibits NF-κB-BRD4 binding by scavenging BRD4, leading to an impact on CSF2 promoter transcription. Notably, reducing RASD1 expression resulted in a significant increase in CSF2, a target of the NF-κB signaling pathway[23-25]. Since RASD1 differs from most members of the RAS family, it possesses a distinctive feature- a C-terminal extension of approximately 50 amino acids. The presence of this C-terminal extension is crucial for the actions of RASD1; future studies are needed to assess which region of amino acids is involved in these processes.

When RASD1 expression decreased, CSF2 secretion increased that promoting immune activation, which plays a role in suppressing pro-tumor activities. We hypothesize that tumor overexpressing RASD1 are resistant to anti-PD1 therapy. Consistent with this hypothesis, we demonstrated that RASD1 overexpressed tumors are challenging to treat with anti-PD1 alone. However, further studies are needed to investigate how CSF2 functions within immune cells when RASD1 is overexpressed.

The finding that RASD1 promotes the expression of Arg1 and Mrc1 in TAMs suggests that RASD1 may recruit M2 macrophages and regulate macrophage switching and pro-tumor immunity in tumor microenvironment. This additional possibility, where

CSF2 receptor expression decreases in RASD1-overexpressed TAMs, will be investigated in future studies.

A recent report has identified CSF2 as a pro-inflammatory cytokine widely utilized in clinical settings. We propose CSF2 as a therapeutic strategy to target RASD1. CSF2 can switch macrophages to a pro-inflammatory phenotype when RASD1 is overexpressed. However, using CSF2 alone shows limited therapeutic efficacy. Therefore, we suggest CSF2 and anti-PD1 combination treatment to treat RASD1 overexpressed tumors. The analysis of immune cells from RASD1-overexpressed tumors treated with the combination therapy revealed an increased in the infiltration of proinflammatory M1 macrophages and decrease in immunosuppressive M2 macrophages. Given that we successfully observed therapeutic effect in tumors overexpressing RASD1 with combination immunotherapy, further research is needed in future clinical studies, particularly regarding the reaction of CSF2.

Efforts to identify predictive biomarkers for immunotherapy response have intensified, with ongoing exploration for a deeper and more comprehensive understanding in recent years. Through multiple approaches, we confirmed RASD1 as a cancer immunotherapy biomarker. Our analysis revealed elevated RASD1 expression in gastric cancer patient tissue treated with immunotherapy, demonstrating that RASD1 can role as a diagnostic marker. These findings, along with our work, suggest that RASD1 expression can provide clinically impactful information to guide therapy.

Our study has translational potential, given that RASD1 is highly expressed in chemo-resistant mesenchymal cancer cells as it serves as a target gene for GR. Increased RASD1 expression is associated with tumor growth and resistance to immune checkpoint inhibitors. Additionally, we evaluated the immune score using bulk RNA sequencing data from gastric cancer patients and found that high RASD1 expression in the non-responder group lacked M1 macrophages. However, further study is needed to determine whether

cytotoxic T cells have not changed significantly. We propose macrophage-targeted immunotherapy as a potential approach to treat RASD1-overexpressed tumors by targeting CSF2. Additionally, we uncovered a potential role of RASD1 in suppressing immune checkpoint blockade responses in gastric cancer patients. The role of RASD1 as a biomarker for immunotherapy sensitivity requires further investigation in human gastric cancer patients, and future studies are needed to address the role of RASD1 in patients suffering from other immunotherapy- resistant cancers.

Our study will motivate new line of investigations as it provides a rational mechanistic basis to design novel GR signaling target gene and immunotherapy combinatorial therapeutic strategies to determine the clinical antitumor effect in ICI-resistant cancer patients.

V. CONCLUSION

In this study, we elucidated that RASD1, a target gene of GR signaling pathway, act as a key mediator of immune suppression, influencing immunotherapy response and serving as a potential biomarker. Transcriptomic analysis of gastric cancer cells reveals that RASD1 downregulation enhances the anti-tumor immune response. Ablation of RASD1 upregulates CSF2, a target gene of NF-κB signaling pathway. Through an in vivo study using a syngeneic mouse model, we found RASD1 expression in cancer cells correlates with larger tumor size and resistance to ICB. Additionally, in gastric cancer patient immunotherapy cohorts, elevated RASD1 expression is correlated with poor ICB results. This is because RASD1 interacts with BRD4, thereby suppressing CSF2 transcription and NF-κB signaling pathway activation. In conclusion, we suggest RASD1 emerges as a promising biomarker for distinguishing immunotherapy responder from non-responders.

PUBLICATION LIST

1. Bray F, Ferlay J, Soerjomataram I, Siegel RL, Torre LA, Jemal A. Global cancer statistics 2018: GLOBOCAN estimates of incidence and mortality worldwide for 36 cancers in 185 countries. CA Cancer J Clin 2018;68:394-424.
2. Cunningham D, Allum WH, Stenning SP, Thompson JN, Van de Velde CJ, Nicolson M, et al. Perioperative chemotherapy versus surgery alone for resectable gastroesophageal cancer. N Engl J Med 2006;355:11-20.
3. Al-Batran SE, Homann N, Pauligk C, Goetze TO, Meiler J, Kasper S, et al. Perioperative chemotherapy with fluorouracil plus leucovorin, oxaliplatin, and docetaxel versus fluorouracil or capecitabine plus cisplatin and epirubicin for locally advanced, resectable gastric or gastro-oesophageal junction adenocarcinoma (FLOT4): a randomised, phase 2/3 trial. Lancet 2019;393:1948-57.
4. Cheong J-H, Yang H-K, Kim H, Kim WH, Kim Y-W, Kook M-C, et al. Predictive test for chemotherapy response in resectable gastric cancer: a multi-cohort, retrospective analysis. The Lancet Oncology 2018;19:629-38.
5. Lauren P. THE TWO HISTOLOGICAL MAIN TYPES OF GASTRIC CARCINOMA: DIFFUSE AND SO-CALLED INTESTINAL-TYPE CARCINOMA. AN ATTEMPT AT A HISTO-CLINICAL CLASSIFICATION. Acta Pathol Microbiol Scand 1965;64:31-49.
6. Kim N. Sex/Gender-Specific Medicine for Intestinal-Type and Diffuse-Type Gastric Cancer. In: Kim N, editor. Sex/Gender-Specific Medicine in the Gastrointestinal Diseases. Singapore: Springer Nature Singapore; 2022. p.153-68.
7. Cha JY, Kim HJ, Yu JH, Xu J, Kim D, Paul BD, et al. Dexras1 mediates glucocorticoid-associated adipogenesis and diet-induced obesity. Proceedings of the National Academy of Sciences 2013;110:20575-80.
8. Seok JW, Kim D, Yoon BK, Lee Y, Kim HJ, Hwang N, et al. Dexras1 plays a pivotal role in maintaining the equilibrium between adipogenesis and osteogenesis. Metabolism 2020;108:154250.
9. Kim HJ, Cha JY, Seok JW, Choi Y, Yoon BK, Choi H, et al. Dexras1 links glucocorticoids to insulin-like growth factor-1 signaling in adipogenesis. Scientific Reports 2016;6:28648.
10. Balwierz PJ, Pachkov M, Arnold P, Gruber AJ, Zavolan M, van Nimwegen E. ISMARA: automated modeling of genomic signals as a democracy of regulatory motifs. Genome Res 2014;24:869-84.
11. Kim J, Park C, Kim KH, Kim EH, Kim H, Woo JK, et al. Single-cell analysis of

gastric pre-cancerous and cancer lesions reveals cell lineage diversity and intratumoral heterogeneity. npj Precision Oncology 2022;6:9.
12. Yoon Bo K, Kim H, Oh Tae G, Oh Se K, Jo S, Kim M, et al. PHGDH preserves one-carbon cycle to confer metabolic plasticity in chemoresistant gastric cancer during nutrient stress. Proceedings of the National Academy of Sciences 2023;120:e2217826120.
13. Méndez-Samperio P. Expression and regulation of chemokines in mycobacterial infection. J Infect 2008;57:374-84.
14. Wu Y, Li YY, Matsushima K, Baba T, Mukaida N. CCL3-CCR5 axis regulates intratumoral accumulation of leukocytes and fibroblasts and promotes angiogenesis in murine lung metastasis process. J Immunol 2008;181:6384-93.
15. Watts TH. TNF/TNFR family members in costimulation of T cell responses. Annu Rev Immunol 2005;23:23-68.
16. Brasier AR, Tian B, Jamaluddin M, Kalita MK, Garofalo RP, Lu M. RelA Ser276 phosphorylation-coupled Lys310 acetylation controls transcriptional elongation of inflammatory cytokines in respiratory syncytial virus infection. Journal of Virology 2011;85:11752-69.
17. Tian B, Yang J, Zhao Y, Ivanciuc T, Sun H, Garofalo RP, et al. BRD4 Couples NF-κB/RelA with Airway Inflammation and the IRF-RIG-I Amplification Loop in Respiratory Syncytial Virus Infection. Journal of Virology 2017;91:10.1128/jvi.00007-17.
18. Hayden MS, Ghosh S. NF-κB in immunobiology. Cell Res 2011;21:223-44.
19. Ashburner BP, Westerheide SD, Baldwin AS, Jr. The p65 (RelA) subunit of NF-kappaB interacts with the histone deacetylase (HDAC) corepressors HDAC1 and HDAC2 to negatively regulate gene expression. Mol Cell Biol 2001;21:7065-77.
20. Huang B, Yang XD, Zhou MM, Ozato K, Chen LF. Brd4 coactivates transcriptional activation of NF-kappaB via specific binding to acetylated RelA. Mol Cell Biol 2009;29:1375-87.
21. Zhong H, May MJ, Jimi E, Ghosh S. The Phosphorylation Status of Nuclear NF-KB Determines Its Association with CBP/p300 or HDAC-1. Molecular Cell 2002;9:625-36.
22. LeRoy G, Rickards B, Flint SJ. The Double Bromodomain Proteins Brd2 and Brd3 Couple Histone Acetylation to Transcription. Molecular Cell 2008;30:51-60.
23. Karin M. Nuclear factor-κB in cancer development and progression. Nature 2006;441:431-6.
24. Taniguchi K, Karin M. NF-κB, inflammation, immunity and cancer: coming of age. Nature Reviews Immunology 2018;18:309-24.
25. Metcalf D. The molecular biology and functions of the

granulocyte-macrophage colony-stimulating factors. Blood 1986;67:257-67.
26. Inaba K, Inaba M, Romani N, Aya H, Deguchi M, Ikehara S, et al. Generation of large numbers of dendritic cells from mouse bone marrow cultures supplemented with granulocyte/macrophage colony-stimulating factor. J Exp Med 1992;176:1693-702.
27. Nebiker CA, Han J, Eppenberger-Castori S, Iezzi G, Hirt C, Amicarella F, et al. GM-CSF Production by Tumor Cells Is Associated with Improved Survival in Colorectal Cancer. Clin Cancer Res 2014;20:3094-106.
28. Cheever MA, Higano CS. PROVENGE (Sipuleucel-T) in prostate cancer: the first FDA-approved therapeutic cancer vaccine. Clin Cancer Res 2011;17:3520-6.
29. Dranoff G, Jaffee E, Lazenby A, Golumbek P, Levitsky H, Brose K, et al. Vaccination with irradiated tumor cells engineered to secrete murine granulocyte-macrophage colony-stimulating factor stimulates potent, specific, and long-lasting anti-tumor immunity. Proc Natl Acad Sci U S A 1993;90:3539-43.
30. Zhu H, Kauffman ME, Trush MA, Jia Z, Li YR. A Simple Bioluminescence Imaging Method for Studying Cancer Cell Growth and Metastasis after Subcutaneous Injection of Lewis Lung Carcinoma Cells in Syngeneic C57BL/6 Mice. React Oxyg Species (Apex) 2018;5:118-25.
31. Partecke LI, Sendler M, Kaeding A, Weiss FU, Mayerle J, Dummer A, et al. A Syngeneic Orthotopic Murine Model of Pancreatic Adenocarcinoma in the C57/BL6 Mouse Using the Panc02 and 6606PDA Cell Lines. European Surgical Research 2011;47:98-107.
32. Jungwirth U, van Weverwijk A, Melake MJ, Chambers AF, Gao Q, Fivaz M, et al. Generation and characterisation of two D2A1 mammary cancer sublines to model spontaneous and experimental metastasis in a syngeneic BALB/c host. Disease Models & Mechanisms 2018;11.
33. Jin S, Guerrero-Juarez CF, Zhang L, Chang I, Ramos R, Kuan CH, et al. Inference and analysis of cell-cell communication using CellChat. Nat Commun 2021;12:1088.
34. Kitamura T, Qian BZ, Soong D, Cassetta L, Noy R, Sugano G, et al. CCL2-induced chemokine cascade promotes breast cancer metastasis by enhancing retention of metastasis-associated macrophages. J Exp Med 2015;212:1043-59.
35. Ma RY, Zhang H, Li XF, Zhang CB, Selli C, Tagliavini G, et al. Monocyte-derived macrophages promote breast cancer bone metastasis outgrowth. J Exp Med 2020;217.
36. Qian BZ, Li J, Zhang H, Kitamura T, Zhang J, Campion LR, et al. CCL2 recruits inflammatory monocytes to facilitate breast-tumour metastasis.

Nature 2011;475:222-5.
37. Qian B-Z, Pollard JW. Macrophage Diversity Enhances Tumor Progression and Metastasis. Cell 2010;141:39-51.
38. Mantovani A, Marchesi F, Malesci A, Laghi L, Allavena P. Tumour-associated macrophages as treatment targets in oncology. Nature Reviews Clinical Oncology 2017;14:399-416.
39. Robinson A, Han CZ, Glass CK, Pollard JW. Monocyte Regulation in Homeostasis and Malignancy. Trends Immunol 2021;42:104-19.
40. Mantovani A, Marchesi F, Jaillon S, Garlanda C, Allavena P. Tumor-associated myeloid cells: diversity and therapeutic targeting. Cell Mol Immunol 2021;18:566-78.
41. Qorraj M, Bruns H, Böttcher M, Weigand L, Saul D, Mackensen A, et al. The PD-1/PD-L1 axis contributes to immune metabolic dysfunctions of monocytes in chronic lymphocytic leukemia. Leukemia 2017;31:470-8.
42. Georgoudaki A-M, Prokopec Kajsa E, Boura Vanessa F, Hellqvist E, Sohn S, Östling J, et al. Reprogramming Tumor-Associated Macrophages by Antibody Targeting Inhibits Cancer Progression and Metastasis. Cell Reports 2016;15:2000-11.
43. Park S, Karalis JD, Hong C, Clemenceau JR, Porembka MR, Kim I-H, et al. ACTA2 Expression Predicts Survival and Is Associated with Response to Immune Checkpoint Inhibitors in Gastric Cancer. Clinical Cancer Research 2023;29:1077-85.

ABSTRACT(IN KOREAN)

종양 내 RASD1에 의한 항-종양 면역 억제기전

<지도교수 황성순>

연세대학교 대학원 의과학과

전규혜

위암은 전세계 암 사망 중 세 번째로 높은 사망률을 기록하는 질병이다. 조기 치료 시 생존율은 높지만, 국소전이가 일어난 위암은 5년 생존율이 6.7%로 급격히 낮아진다. 이러한 국소전이 위암은 항암제가 잘 듣지 않아 치료를 위한 전략이 필요하다. 위암의 아형 중 줄기세포형 아형은 면역반응이 잘 일어나지 않고 항암제에 저항성을 가지고 있어 생존율이 낮은 것으로 알려져 있다. 본 연구는 당질코르티코이드 수용체가 면역반응 억제를 유도하는 특성과 줄기세포형 아형을 연관 지어 연구를 진행하였다. RASD1은 합성 당질코르티코이드인 덱사메타손에 의해 유도되는 RAS 단백질이다. 본 연구는 RASD1이 위암 내 면역 반응 억제 역할을 하며, RASD1 발현을 억제할 경우 암세포의 염증반응이 증가한다는 것을 보여주었다. 또한 RASD1 발현이 증가되어 있는 종양은 크기가 더 커지고 면역항암제에 저항성을 갖는다는 것을 확인하였다. 암 세포에서 RASD1 발현이 감소하면 전-염증성 사이토카인 CSF2 분비가 증가하며, 이를 토대로 RASD1이 과발현된 종양의 치료방법으로 CSF2와 면역항암제를 병용 투여했을 때 종양의 크기가 줄어드는 것을 확인할 수 있었다. 또한 RASD1의 면역 억제 기전은 BRD4와 상호작용하여 NF-κB의 염증반응 신호를 억제한다는 것을 밝혀냈다. 더 나아가, 면역항암제를 투여한 위암 환자 중 면역 항암제 비반응군의 RASD1발현이 반응군에 비해 유의미하게 증가되어 있는 것을 확인할 수 있었다. 이는 RASD1이 면역 치료 예후에 대한 생체 표지로 작용할 수 있다는 점을 시사한다. 본 연구를 통해 RASD1 발현이 증가되어 있는 환자는 예후가 좋지 않고, RASD1이 개인 맞춤형 치료에 기여할 수 있는 마커로

작용할 수 있다는 것을 제시하였다.

핵심되는 말 : 위암, 라스디1, 면역 억제, 면역치료, 생체표지